

Review

Recent Advances in the Synthesis of Metal Oxide Nanofibers and Their Environmental Remediation Applications

Kunal Mondal

Department of Chemical and Biomolecular Engineering, North Carolina State University, 911 Partners Way, Raleigh, NC 27695, USA; kmondal@ncsu.edu; Tel.: +1-919-260-9449

Academic Editors: Mallikarjuna N. Nadagouda, Hyuksang Chang and Changseok Han

Received: 20 March 2017; Accepted: 26 May 2017; Published: 1 June 2017

Abstract: Recently, wastewater treatment by photocatalytic oxidation processes with metal oxide nanomaterials and nanocomposites such as zinc oxide, titanium dioxide, zirconium dioxide, etc. using ultraviolet (UV) and visible light or even solar energy has added massive research importance. This waste removal technique using nanostructured photocatalysts is well known because of its effectiveness in disintegrating and mineralizing the unsafe organic pollutants such as organic pesticides, organohalogens, PAHs (Polycyclic Aromatic Hydrocarbons), surfactants, microorganisms, and other coloring agents in addition to the prospect of utilizing the solar and UV spectrum. The photocatalysts degrade the pollutants using light energy, which creates energetic electron in the metal oxide and thus generates hydroxyl radical, an oxidative mediator that can oxidize completely the organic pollutant in the wastewater. Altering the morphologies of metal oxide photocatalysts in nanoscale can further improve their photodegradation efficiency. Nanoscale features of the photocatalysts promote enhance light absorption and improved photon harvest property by refining the process of charge carrier generation and recombination at the semiconductor surfaces and in that way boost hydroxyl radicals. The literature covering semiconductor nanomaterials and nanocomposite-assisted photocatalysis—and, among those, metal oxide nanofibers—suggest that this is an attractive route for environmental remediation due to their capability of reaching complete mineralization of organic contaminants under mild reaction conditions such as room temperature and ambient atmospheric pressure with greater degradation performance. The main aim of this review is to highlight the most recent published work in the field of metal oxide nanofibrous photocatalyst-mediated degradation of organic pollutants and unsafe microorganisms present in wastewater. Finally, the recycling and reuse of photocatalysts for viable wastewater purification has also been conferred here and the latest examples given.

Keywords: metal oxide nanofiber; nanofiber photocatalyst; electrospun nanofibers; photocatalysis; wastewater treatment; UV light; visible light photocatalysis; solar energy; photocatalytic reactor; water disinfection; recycling of photocatalyst

1. Introduction

For the treatment of agricultural and industrial wastewater that contains traces of refractory organic compounds such as organic pesticides, surfactants, organohalogens, and coloring agents, wastewater purification technologies are now essential to build economical and more advanced treatment methods. In general, a combination of several approaches gives high treatment efficiency compared with existing treatments. For example, a certain pollutant can hardly be degraded by photolysis with conventional photocatalysts in the ambient environment and treated wastewater may need more steps for total mineralization [1–4]. However, a combination of several methods, such as

synthesizing suitable nanostructured catalysts and optimizing the wavelength of light exposure depending on the selection semiconductor material with favorable bandgap energy, improves the degradation of pollutants from the wastewater [5–7].

On the other hand, photocatalysis has an enormous potential for the elimination of organic pollutants from wastewater [6,8–10]. However, it is still not in practical use since it has a low oxidation rate. Therefore, a combination of selection of photocatalysts together with light source, which can boost oxidation, is reasonable for the management of hard-to-decompose organic pollutants. The challenging organic pollutants are then expected to decompose more rapidly and thoroughly in the presence of a suitable photocatalyst along with an appropriate light source.

In a broad sense, environmental remediation includes the elimination of agricultural, industrial pollutants, hard-to-decompose organic compounds, bacteria, germs, and fungus present in wastewater, along with cleansing of air pollutants such as volatile organic compounds (VOCs) and nitrogen di-oxide (NO_x). Figure 1 illustrates the idea of environmental remediation using photocatalysis.

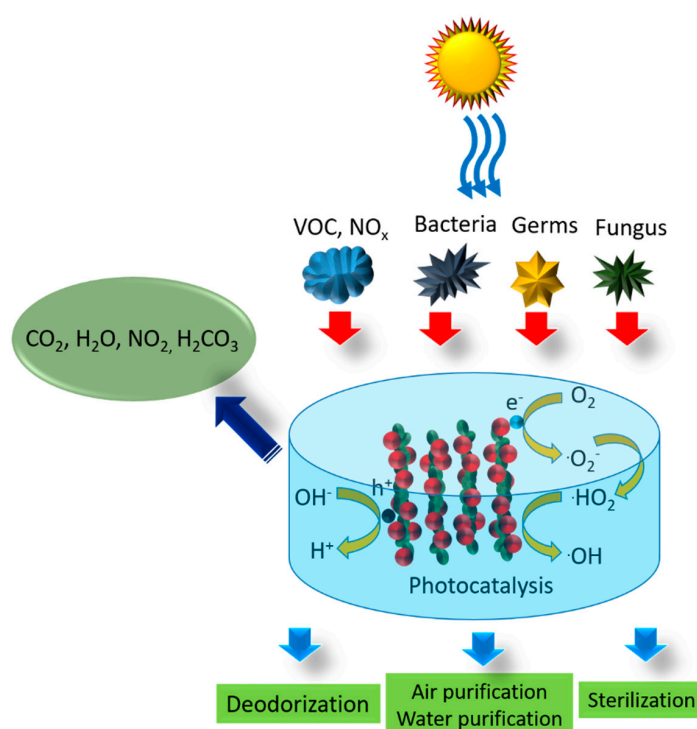


Figure 1. Schematic for the representation of environmental remediation by photocatalysis.

Last year, Anjum et al. [11] published a comprehensive review article on environmental remediation using different nanomaterials. It is clear from their perspective that electrospun nanofibers and other hybrid nano-membranes are very effective for the efficient removal of organic dyes, heavy metals, and foulants. In a recent study, radially oriented ZnO nanowires were decorated on flexible poly-L-lactide nanofibers for continuous-flow photocatalytic water purification [12]. The photocatalytic decomposition was monitored on various organic pollutant dyes, such as methylene blue, monocrotophos, and diphenylamine under illumination with UV light using this highly flexible hierarchical nanostructure. The same electrospun ZnO- poly-L-lactide nanofibers photocatalysts have been used for the adsorption of Cr(VI) as a crucial step for water purification by Burks et al. [13].

The main objective of this paper is to review the most recently published work in the field of ultraviolet- and visible-light-driven photocatalysis on wastewater treatment. The summary of photocatalytic degradation pollutant dyes, bacteria containing wastewater, and volatile organic compounds (VOC) in air degraded by various researchers using metal oxide nanofibers, including

information about the synthesis routes of different sizes of fibers, is presented in Table 1. All results using different organic effluents showed that the application of photocatalysis led to efficient and complete degradation and produced simple products that are environmentally safe; however, incomplete mineralization can result in the formation of highly toxic byproducts.

Table 1. Table of metal oxide nanofiber photocatalysts and their environmental remediation applications.

Nanofibers	Fiber Diameter (nm)	Fabrication Method	Light Irradiated	Application	Literature
ZnO	50–150	Electrospinning	UV	Photocatalysis of PAH dyes	Singh et al. [14]
Carbon doped TiO ₂	25–75	Electrospinning	UV	Photocatalysis of PAH dyes	Mondal et al. [15]
Al ₂ O ₃ –ZrO ₂ /TiO ₂	150–200	Sol–gel synthesis	UV	Photocatalysis of methyl orange and methylene blue	Hong et al. [16]
C/TiO ₂	30–50	Electrospinning	UV	Photocatalysis of methyl orange	Reddy et al. [17]
CdS/TiO ₂	100–140	Electrospinning	UV and visible	Photocatalysis of para-nitrophenol dye	Singh et al. [18]
ZnO/Zn(OH)F	~100	Microfluidic chemical method	UV	Photocatalysis of methylene blue and histidine-rich protein separation	Zhao et al. [19]
Ce _{1-x} Zr _x O ₂ /SiO ₂	50–80	Carbon nanofiber (CNF) template-assisted alcohol-thermal procedure	UV	Photocatalysis of methylene blue	Zhang et al. [20]
Al ₂ O ₃ -Mn ₃ O ₄	~200	Low-temperature stirring	Visible	Photocatalysis of brilliant cresyl blue	Asif et al. [21]
carbon/MWCNT/Fe ₃ O ₄	100–150	Electrospinning	UV	Simultaneous photocatalysis of phenol and paracetamol	Akhi et al. [22]
TiO ₂	50–200	Electrospinning-alkali-acid” combined method.	UV	Photocatalysis of rhodamine B and improved supercapacitance	Wang et al. [23]
graphitic carbon nitride (g-C ₃ N ₄)	~200	Electrospinning and subsequent hydrothermal treatment	Visible solar	Photocatalysis of antibiotics	Qin et al. [24]
CNT/TiO ₂	266–292	Electrospinning	UV and visible	Photocatalysis of benzene (gas phase), methylene blue	Wongaree et al. [25]
SiO ₂ –Bi ₂ WO ₆	430	Electrospinning Soaking and calcination	UV and visible	Photocatalysis of rhodamine B	Ma et al. [26]
SiO ₂ /CuO	300	Electrospinning Soaking and calcination	UV and visible	Photocatalysis of rhodamine B degradation	Hu et al. [27]
RGO/InVO ₄	250–400	Electrospinning	Visible	Photocatalysis of rhodamine B	Ma et al. [28]
Ag ₃ PO ₄ /TiO ₂	100–200	Electrospinning and solution processes	Visible	Photocatalysis of rhodamine B	Xie et al. [29]
WO ₃	80–100	Electrospinning	Visible	Photocatalysis of methylene blue	Ofori et al. [30]
Fe ₃ O ₄ /TiO ₂ /Ag	10	Sol–gel, hydrothermal method, photoreduction	UV and visible	Photocatalysis of Ampicillin	Zhao et al. [31]
TiO ₂ /ZnS–In ₂ S ₃	130	Electrospinning, hydrothermal method	Visible	Photocatalysis of rhodamine B	Liu et al. [32]
PAN-ZnO/Ag	702–998	Single-capillary electrospinning, hydrothermal, and reduction	UV	Photocatalysis of methylene blue	Chen et al. [33]

Table 1. Cont.

Nanofibers	Fiber Diameter (nm)	Fabrication Method	Light Irradiated	Application	Literature
TiO ₂ / ZnFe ₂ O ₄	200–300	Hydrothermal	UV and visible	Photo-electrochemical activity	Liang et al. [34]
BiOCl/Bi ₄ Ti ₃ O ₁₂	80	Electrospinning technique and solvothermal method	Visible	Photocatalysis of methyl orange and para-nitrophenol	Zhang et al. [35]
ZnO/nickel phthalocyanine	610	Two-step hydrothermal approach	Visible	Photocatalysis of rhodamine B assisted by H ₂ O ₂	Wang et al. [36]
Polyaniline/CaCu ₃ Ti ₄ O ₁₂	30–50	In-situ polymerization	Visible	Photocatalysis of methyl orange, congo red dyes	Kushwaha et al. [37]
Cellulose/TiO ₂ / tetracycline (TC) and phosphomycin	3.5	Green chemistry approach	UV	Antibacterial and photochemical application towards pathogen microorganisms: <i>Staphylococcus aureus</i> and <i>Escherichia coli</i>	Galkina et al. [38]
ZnO	678	Electrospinning, hydrolysis	UV	Photocatalysis of methyl orange	Liu et al. [39]
carbon nanotube/TiO ₂	~300	Combined sol–gel and electrospinning technique	UV and visible	Indoor benzene, toluene, ethyl benzene and o-xylene (BTEX) purification	Kang et al. [40]
CNT-TiO ₂	~300	Electrospinning method coupled to hydrothermal treatment	UV and visible	Oxidation of toluene and isopropyl alcohol	Kang et al. [41]
polyamide 6, polystyrene, polyurethane/TiO ₂	107–350	Electrospinning	Visible	Nitrogen oxide (NO _x) removal in air purification	Szatmáry et al. [42]
S-doped TiO ₂	2000–4000	Electrospinning	Visible	Rhodamine B degradation	Ma et al. [43]
polyaniline-coated TiO ₂ /SiO ₂	~500	Electrospinning, calcination and in situ polymerization	Visible	Photocatalysis of methyl orange degradation	Liu et al. [44]
p-MoO ₃ Nanostructures/n-TiO ₂	~300	Electrospinning method coupled to hydrothermal treatment	UV	Photocatalysis of rhodamine B	Lu et al. [45]
TiO ₂ /carbon/ Ag	250–350	Electrospinning technique and hydrothermal	Visible	Photocatalysis of rhodamine B and methyl orange	Zhang et al. [46]
ZnO–Carbon	400–500	Electrospinning technique and hydrothermal	UV	Photocatalysis of rhodamine B	Mu et al. [47]

2. Nanofibers

There is a serious disadvantage to nanoparticles: very often they become agglomerated while dispersed in an aqueous medium and the macroscopic properties are compromised [48,49]. However, nanofibers overcome this problem owing to their fibrous form [50]. In addition, the nanoscopic dimension naturally provides a high surface area to volume ratio. This characteristic makes them very attractive in applications where large surface area is necessary [51]. Nanofibers are different to nanoparticles in terms of aspect ratios and not the same as nanotubes because of crystallographic properties. A fibrous morphology is beneficial over a particle morphology in several respects, e.g., the mechanism of photocatalysis, the function of noble metal, the heterojunctions, and the plasmonic properties.

Solid nanofibers with diameters in the submicron to nanometer range can be synthesized from various polymers and consequently have different physicochemical properties and application possibilities. Polymer chains in a nanofiber are associated via a covalent interaction [52]. Nanofibers are distinctive owing to their flexibility in surface functionalization compared to their microfibers, good mechanical strength, high porosity, and enormous surface area-to-volume ratio, etc. [53]. There exist many natural polymeric nanofibers including, gelatin, cellulose, silk fibroin, collagen, keratin, alginate, chitosan, etc., and synthetic polymers such as polycaprolactone (PCL), poly(lactic acid) (PLA), poly(lactic-co-glycolic acid) (PLGA), poly(ethylene-co-vinylacetate) (PEVA), polyurethane (PU), poly(3-hydroxybutyrate-co-3-hydroxyvalerate) (PHBV), etc. [54].

The diameters of nanofibers are mainly determined by the nature of the precursor polymer used, the parameters involved, and the method of fabrication [55]. There are various methods used to synthesize nanofibers, including electrospinning, dry spinning, thermal-induced phase separation, self-assembly, drawing, extrusion, template synthesis, etc. [56]. Among these, electrospinning is the most frequently used technique to produce nanofibers. It has many advantages such as simple and straightforward setup, easy mass production of continuous nanofibers from numerous polymers, and, most interestingly, the ability to produce ultrathin fibers with tunable diameters, compositions, and alignments [57]. This flexibility permits the shape controllability and organization of the fibers on any collector or even in the form of free-standing fibers so that many different structures such as hollow, core-shell, flat ribbon, and even spherical particles shaped by electrospinning can be fabricated on demand to meet the desired application requirements [58–60]. Those special nanofiber structures and textures can be exploited in various advanced applications such as energy storage, gas sensors and biosensors, nanofluidics, catalysis and photocatalysis, drug delivery and release, catalytic nano supports, etc. [61–66].

3. Electrospinning

The electrospinning method offers a straightforward electrohydrodynamical mechanism [67–69] to yield fibers with diameters measuring less than 100 nm [70], even up to 10 nm [71]. Widespread exploration has been done on the electrospinning technique to fabricate nanofibers [72]. Based on the reported literature, the basic electrospinning setup (shown in Figure 2) essentially involved three key parts: a syringe with a metallic needle having a suitable polymeric melt, a high-voltage power supply, and a conducting collector with an adjustable configuration. The process of fabrication of the nanofiber starts when electrically charged particles travel into the polymeric melt through the metallic needle. This originates instability within the polymeric melt because of the induction of electrically charged particles on the polymer drop. Simultaneously, the mutual repulsive force of charged particles originates an electrical force that competes with the surface tension of the polymer, and finally the polymer melt proceeds in the direction of the electric force. An additional escalation in the electric field causes the spherical shaped droplet that emerges from the needle to distort and take on a conical shape. A static or rotating collector assembly, electrically grounded and kept at an optimal distance, collects the ultrafine nanofibers from the conical shaped droplet of the polymeric melt (Taylor cone) because of the high electrical field applied. A steady charged polymer jet from the needle to the collector can be formed only when the polymeric melt has enough cohesive force. Throughout the process, the internal (on the fiber) and external (applied electric field) forces on the charged particles cause the whipping motion of the liquid jet towards the collector. Because of this whipping motion, the polymeric chains within the melt stretch and slide past each other, which ultimately results in the form of fibers with diameters measured in the submicron to nanoscale [73,74].

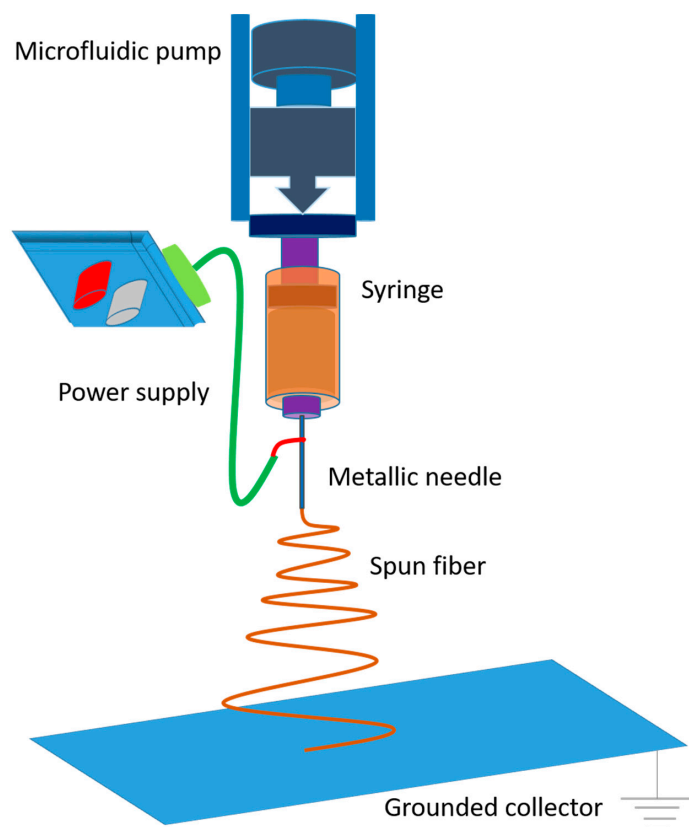


Figure 2. Electrospinning setup for fabricating nanofibers.

4. Core-Shell Nanofibers

The spinnability of a polymeric melt during electrospinning is governed by the viscosity and ionic conductivity solution, and the nature of the solvents, along with the molecular weight and the conformation of the polymer. It is important to note that several polymers are not electrospinnable because of their inadequate solubility in an electrospinning suitable solvent; however, an unspinnable polymer can form nanofibers by co-electrospinning with the help of a spinnable polymer in the same solution [75]. Many dissimilar morphologies of nanofibers, for instance core-shell, hollow, and porous, bi-component structures, could be created with different designs of electrospinning spinnerets and nozzles.

In typical core-shell electrospinning, a coaxial jet is formed by a coaxial nozzle when two dissimilar liquids flow simultaneously through inner and outer capillaries [76]. The free end of the nozzle is connected to a high-voltage electric power supply. The spun nanofibers are consolidated in the course of solvent evaporation and mechanical stretching. The ratio of the solution feeding rate of the two liquid components controls the uniformity and stability of the core and shell flow [77]. Additionally, a few other parameters, such as the applied electric field strength, the shape and size of core-shell capillaries, the volume feed rate of each component, the immiscible nature of the core-shell materials, and their ionic conductivity and viscosity also play an essential role in shaping the uniform formation of core-shell jets and the morphology of the spun nanofibers [78].

5. Hollow and Porous Nanofibers

Hollow nanofibers are targeted for advanced and very specific applications, such as nanofluidics, photocatalysis, solar energy harvest, and hydrogen storage [79]. Typically, two types of techniques, including the direct co-axial spinning method [80] and chemical vapor deposition (CVD) methods, are used for the production of hollow nanofibers [81,82].

To produce hollow nanofibers by the electrospinning method, the co-axial spinning is considered, as shown in Figure 3. In co-axial electrospinning, nanofibers are prepared by following the same process as fabricating core-shell nanofibers; however, the core is removed with a selective solvent etching process at the end of the method [83–85]. For example, poly(vinylpyrrolidone) (PVP) and tetra butyltitanate ($\text{Ti}(\text{OC}_4\text{H}_9)_4$) were electrospun as shell solutions and paraffin oil or mineral oil was poured in as the core material. TiO_2 fibers with a hollow core structure were achieved when the polymer and core materials were removed by selective etching [18]. Figure 4 shows the morphologies of hollow titanium dioxide nanofibers fabricated using the core-shell electrospinning technique, as reported by Sing et al. [18].

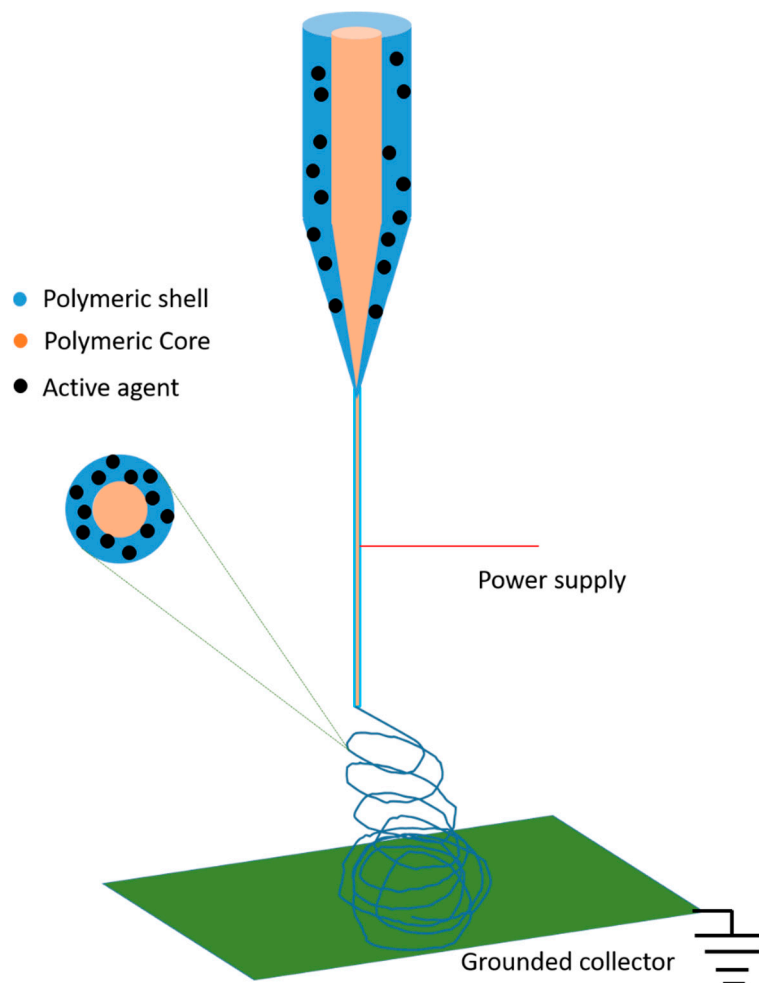


Figure 3. Schematic illustration of the electrospinning setup with two coaxial nozzle for spinning core-shell nanofibers.

In the second CVD method, the first precursor polymer is converted to a nanofiber or a “template” using electrospinning. Then, the spun fibers are coated with either an appropriate polymer or a metal. Lastly, hollow fibers are obtained by removing the template material by selecting solvent etching or by calcining at high temperature in a furnace [83,86–89]. The diameter and morphology of such hollow nanofibers can also be easily tuned by controlling the electrospinning process parameters [83].

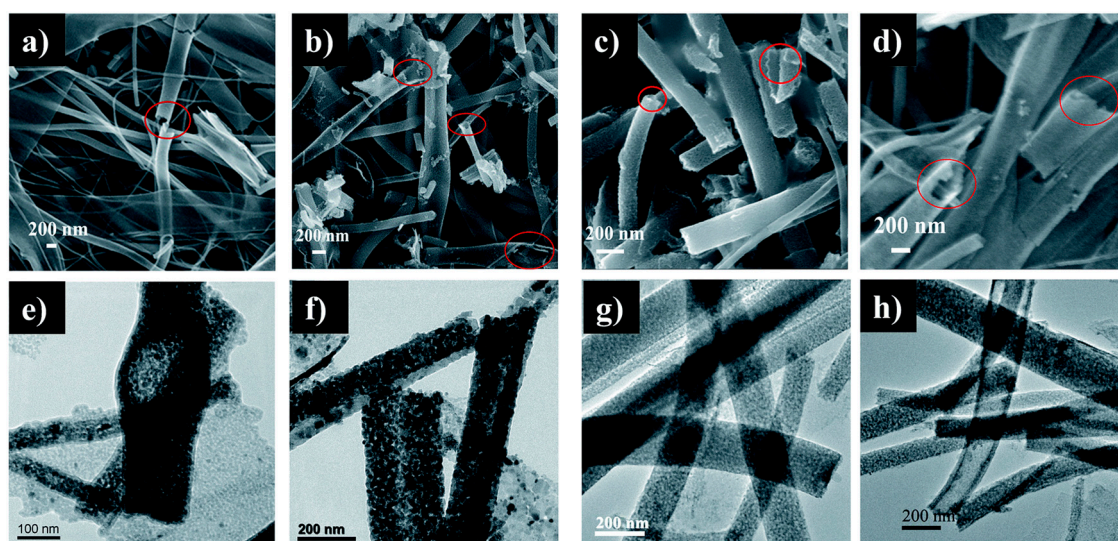


Figure 4. FESEM images (a–d) of CdS loaded TiO₂ hollow nanofibers after different successive ion layer adsorption and reaction (SILAR) cycles (1, 2, 3, and 5), respectively (hollow morphologies of nanofibers can be seen in circular markings); and their TEM micrographs (e–h). Reproduced with permission from [18]. Copyright 2016, Royal Society of Chemistry.

The applicability of porous nanofibers is more comprehensive and broad in contrast with core-shell and hollow nanofibers. Owing to their ultra-high BET surface areas, porous fibers find applications in membranes [90], filtration [91], fuel cells [92], catalysis [93], tissue engineering [94,95], and drug delivery and release [96]. Porous nanofibers can be created with a distinctive topology by choosing precise solvents or a proper mixture of solvents, or polymer mixtures under an optimized environment. One approach could be based on phase separation of the polymeric components in a mixture caused by different evaporation rates. In this method, immiscible polymers are dissolved in a common solvent and electrospun. One of the polymers, either from the core or the shell of the spun fibers, is dissolved to achieve porous nanofibers. There are a few other methods for fabricating porous nanofibers, such as phase separation by vapor, non-solvent and thermally induced phase separation [97–99], rapid phase separation [100,101], selective dissolution [102], and selective calcination [102,103].

6. Metal Oxide Nanofibers

Metal oxide nanofibers have huge research importance for both 1D and 2D nanoscopic morphology due to their exclusive electrical and physicochemical properties. A range of uses has been proven in photovoltaic cells, light-emitting diodes, liquid crystal displays, lithium ion batteries, biosensors, and gas sensors.

There are many methods such as melt, colloid, solution, dry and co-axial electrospinning, CVD, PECVD, and electrochemical methods that are used to yield metal oxide and nanofibers [14,15,104–108]. In recent times, electrospun metal oxides' precursors have garnered much interest for the production of multifunctional nanofibers [109,110]. Figure 5 defines the approach for the synthesis of an electrospun metal oxide nanofiber. There are two ways: either a metal oxide precursor is added to a polymer in the course of electrospinning solution preparation; also, it could be incorporated by dipping spun fibers into a precursor solution afterward.

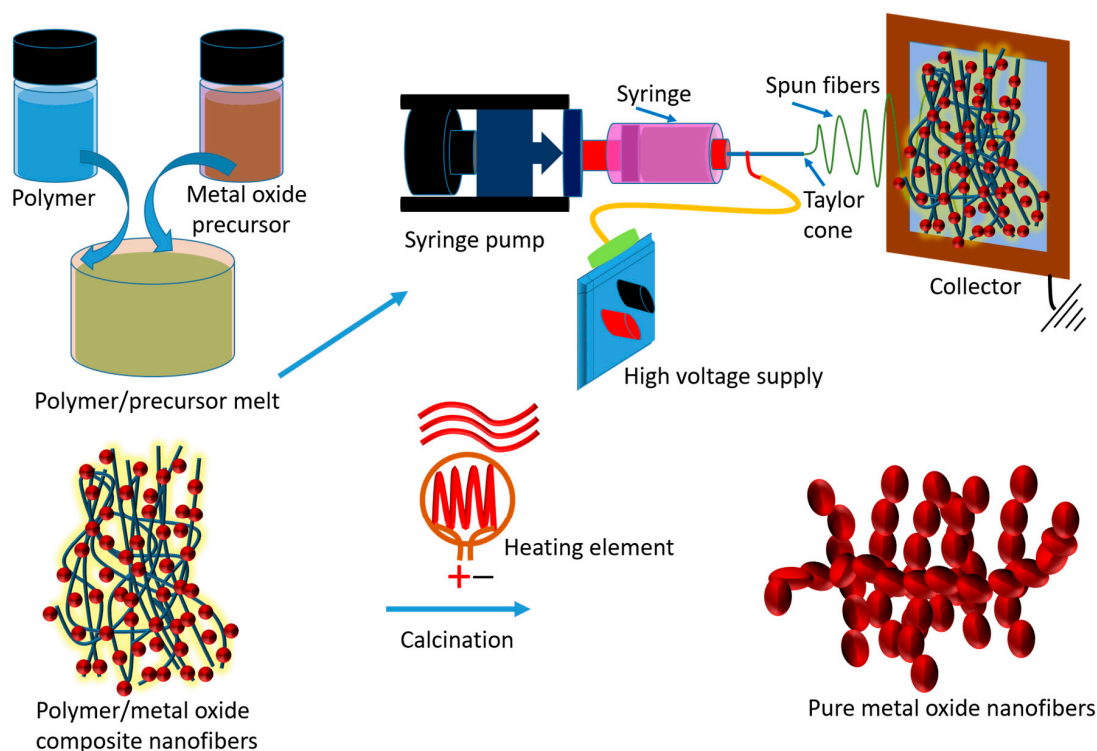


Figure 5. Electrospinning setup for fabrication of metal oxide nanofibers.

Generally, calcination of spun metal oxide nanofibers is a common method for large-scale production. Calcination is a two-step process whereby the polymer is eliminated at high temperature in an oxygen atmosphere and an oxidative conversion of the precursor constituent yields a metal oxide by nucleation and growth at high temperature [111,112].

The metal oxide centers can be incorporated into the nanofiber matrix either in situ or ex situ. A suitable organometallic or sol-gel metal oxide precursor has been introduced with electrospinning polymer melt in situ, whereas soaking nanofibers in a solvent comprising the desired metal oxide precursor produces a surface coating in the latter case. There are many works reported for the electrospinning of metal oxide nanofibers either by the sol-gel route [113–116], or by formation of a polymeric metal oxide colloidal dispersion ex situ [117–119]. In the case of electrospinning from an inorganic precursor, the high-temperature calcination process causes a reduction in the diameter of the fibers as the sacrificial polymer template is selectively removed. Consequently, by reason of calcination, the resultant nanofibers become fragile owing to their thinner cross sections and the thermomechanical stress generated from the reduction in size [105,120–122]. There have been many efforts made in recent times towards the production of metal oxide nanofibers by the electrospinning route. For example, alumina, zinc oxide, silica, and TiO_2 nanoparticles were mixed with the electrospinning polymer solution [118,123–125]. Recently, Sharma's group used a sol-gel precursor of titanium dioxide, titanium isopropoxide, along with a polyvinylpyrrolidone polymer, for electrospinning and fabricated carbon-doped titania nanofibers, as shown in Figure 6 [15].

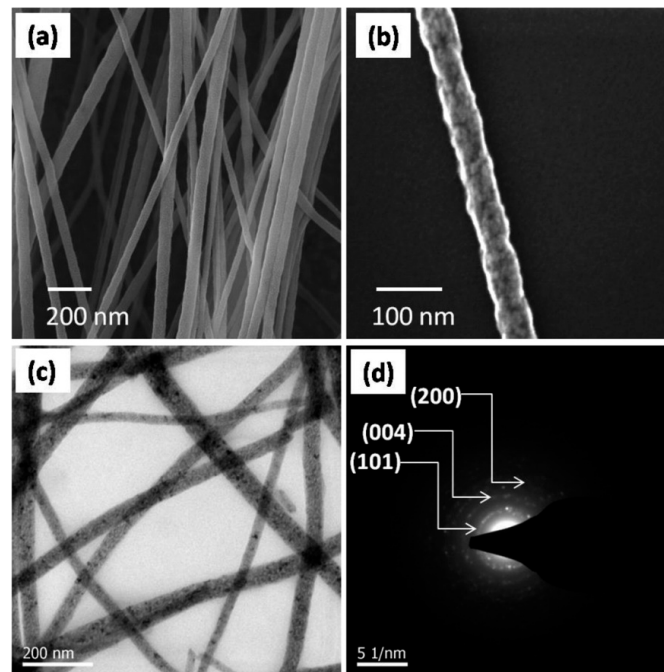


Figure 6. FESEM images of a TiO₂ nanofiber mat produced upon the calcination of PVP/PVP/Ti(OiPr)₄ composite fibers at 500 °C (a); a single titania nanofiber (b); a TEM image of the fibers (c); and a SAED pattern displaying the crystal planes of the anatase phase of TiO₂ (d). The arrows indicate different crystal planes of TiO₂. Reprinted with permission from [15]. Copyright (2014) American Chemical Society.

In another work, ZnO nanofibers were produced using zinc acetate as an inorganic metal oxide precursor along with sacrificial carrier polymer polyacrylonitrile, which was removed during calcination [14]. Figure 7 shows the morphology of the electrospun ZnO nanofibers.

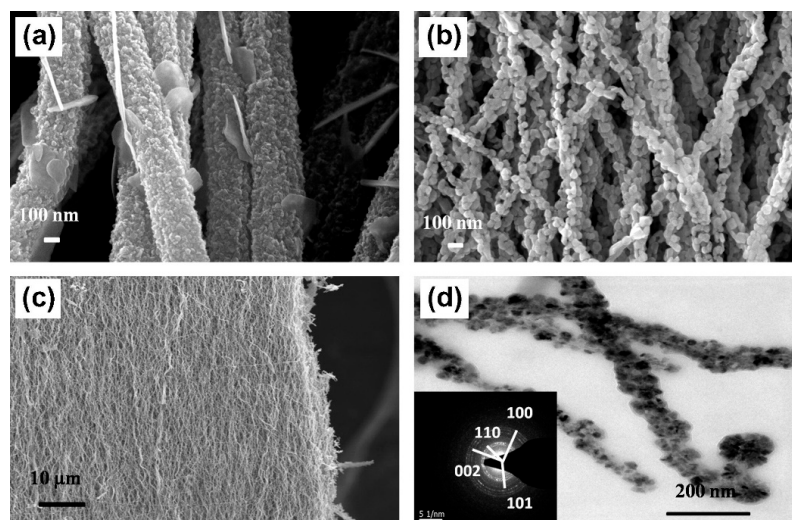


Figure 7. FEEM micrographs of ZnO nanofibers fabricated by calcining at different temperatures: (a) 450 °C; (b) 650 °C; (c) ZnO nanofibers collected in the form of a free standing mat calcined; and (d) a TEM micrograph of ZnO nanofibers and the selected area electron diffraction patterns (SAED) (inset). The arrows indicate different crystal planes of ZnO. Reprinted from [14]. Copyright (2013), with permission from Elsevier.

7. Photocatalysis

Photocatalysis is a potential way to decontaminate amenities, houses, living environments, industrial waste, and numerous organic compounds as well as refractory chlorinated aromatics and more than 27,935 (from Web of Science Core Collection until March 2017) references have been collected on this discipline [126–129]. As compared to other existing chemical oxidation techniques, photocatalysis may be more efficient since semiconductor photocatalysts are economical and can accomplish the complete mineralizing of various refractory compounds [130]. By further adjusting and developing this technology, the pollution in our air and water can be decreased. One can even decrease the spread of pollutions, infections, and disease such as severe acute respiratory syndrome (SARS) in clinics. This purification technology would be an advantage to the whole world.

Serpone and Emiline have argued that photocatalysis is the speeding up of a photoreaction by the action of a catalyst [131]. An earlier IUPAC article defined photocatalysis as a catalytic reaction containing light absorption on a catalyst or a substrate.

Owing to its capability of generating energetic powerful oxidant species, i.e., OH free radicals, photocatalysis can be treated as an advanced oxidation process (AOP). The photochemical AOPs are light-induced reactions, mainly oxidations that depend on the creation of OH[•] by the grouping with supplied oxidants or semiconductor photocatalysts to the system [132]. The photodegradation efficiency of AOPs is significantly improved either by homogeneous or heterogeneous photocatalysis [133]. Heterogeneous photocatalysis hires photocatalyst slurries (for example: ZnO/UV, TiO₂/UV, WO₃, and BiVO₄) for catalysis, while homogeneous photocatalysis (for example: H₂O₂/UV, Fe³⁺/UV) is employed in a single-phase system.

7.1. Mechanism and Kinetics of Photocatalysis by Pure Metal Oxide Nanofibers

The energy difference between the valence band (VB) and the conduction band (CB) in a semiconductor is known as the “Band Gap”. When a metal oxide semiconductor such as TiO₂, ZnO, ZrO₂, SnO₂, CeO₂, etc., absorbs ultraviolet light, it produces an electron–hole pair when the energy is greater than its bandgap energy. The photo-generated electron and hole are negatively and positively charged, respectively. The electron in the conduction band of the photocatalyst gets excited after absorbing photons from light. The electron reacts with an O₂ molecule and yields a superoxide anion. The holes are oxidants, meaning they can oxidize water, which results in the generation of oxygen. The electrons can reduce protons and generate hydrogen. This cycle persists as long as the light energy is accessible.

The chemical reactions in photocatalysis are illuminated as follows with the help of Equations (1)–(9). As ultraviolet light falls on the metal oxide semiconductor photocatalyst, one electron jumps from the valence band to the conduction band, leaving behind a hole. The semiconductors become more efficient if those photo-generated electrons and holes wait before recombining. The electrons in the conduction band react with the O₂ molecule and H⁺ in the surrounding aqueous environment and harvest hydrogen peroxide, which then supplies the OH[−] ion and highly energized OH[•] free radical. Similarly, holes in the valence band react with water to produce an OH[•] free radical. Formation of those highly active species helps to decrease the recombination time of the electron-hole pair and thereby offers extra time for the reaction with the pollutants present in the wastewater. Figure 8 shows the idea of photocatalysis by metal oxide nanofibers through a pictorial illustration.

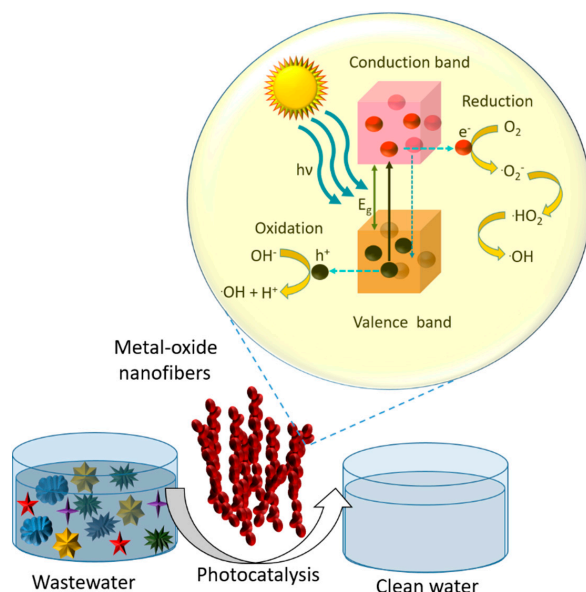
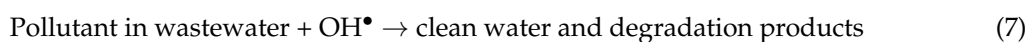


Figure 8. Schematic explanation of the metal oxide semiconductor nanofiber-mediated photocatalysis.

The photocatalytic oxidation of pollutants present in wastewater under ultraviolet light can be described as follows [14]:



The recombination process of the electron–hole pair involves additional energy created from the excited electron, which arises as heat. Since the recombination is undesirable and leads to ineffectual photocatalysis, the key aim of the metal oxide photocatalysts is to produce a catalytic reaction among the conduction band excited electrons and oxidant to yield a reduced product. A reaction among the positively charged holes with a reductant is essential to producing an oxidized product. It is worth mentioning that the reduction and oxidation reactions happen at the nanofiber surface from the time when this reaction generates positive holes and negative electrons. In the oxidative reaction, the hole stands with the moisture content on the fiber surface and returns a hydroxyl free radical. Moreover, if more oxygen is provided, this will act as an electron acceptor and delay the recombination rate, which further enhances the degradation of pollutants [15]. Furthermore, the total time period for pollutant degradation rises with a decrease in nanofiber loading since that will not provide enough reaction sites. Figure 9 shows the typical photocatalysis of polyromantic hydrocarbon (PAH) dye anthracene, which is a pollutant present in wastewater [14]. The fluorescence spectra refer to the gradual degradation of the pollutant by assessing its absorption over time.

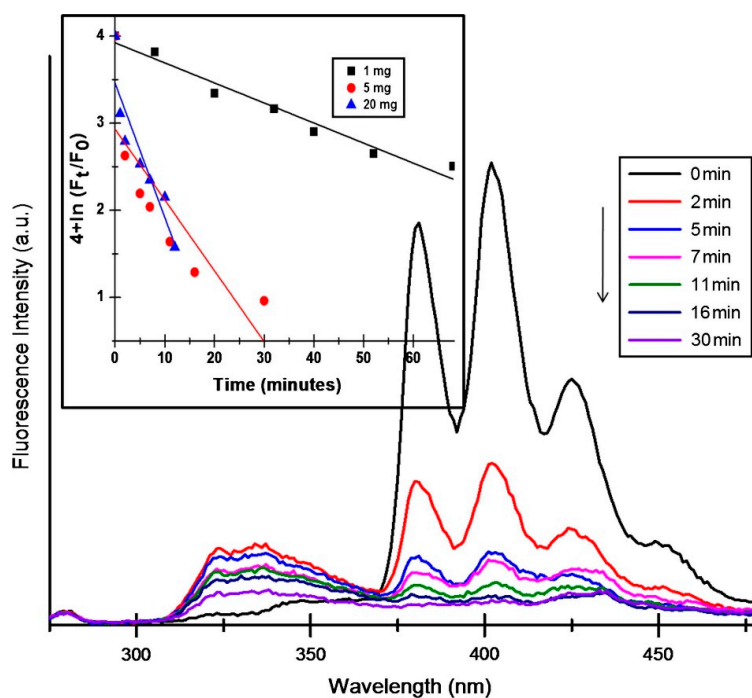


Figure 9. Photocatalytic degradation of anthracene: Fluorescence spectra of 25 ppm anthracene reacted with 5 mg electrospun ZnO nanofibers. The inset shows rate constants for different nanofiber loadings. Reprinted from [14]. Copyright (2013), with permission from Elsevier.

7.2. Mechanisms of Photocatalysis by Metal/Metal Oxide Composite Nanofibers

Metal oxide nanofibers have spurred enormous research interest in photocatalysis as they have the ability to produce charge carriers when exposed to ultraviolet light. The interesting electron bandgap configurations, exceptional light harvest properties, and efficient charge transport characteristics of the metal oxide nanofibers have made them efficient photocatalysts. However, there are some weaknesses in metal oxide photocatalysts, for instance, quick recombination of photogenerated electron–hole pairs and a wide bandgap, which creates the opportunity to fabricate new composite photocatalysts.

The main objective of engineering composite nanofiber photocatalysts is to adjust the photoelectrochemical properties of the metal oxide counterpart and thus a series of metal–metal oxide and metal oxide–metal oxide composite nanofibers have been prepared to simplify charge recombination in the semiconducting nanofibrous nanostructures [134–137]. In this context in a noble metal/metal oxide nanofiber, the metal can act as a sink for photoproduced charge carriers and hence helps with interfacial charge transfer processes in composite photocatalysts during the course of photocatalysis [138]. Figure 10 illustrates the electron transfer process in a metal–metal oxide nanofiber photocatalytic system.

These metal–metal oxide hybrid nanofibers can show characteristics of their singular counterparts or produce completely new properties when these two phases are combined together in composite nanofibers. In an ideal situation, photogenerated charge carriers could be transferred very quickly from one constituent of the composite to the other due to modified electronic band arrangements, thus decreasing the possibility of radiative electron–hole recombination and allowing their use in chemical reactions for longer [139,140]. Additionally, these metal–metal oxide nanofibers, because they can be designed to have several different facets on their surface, create a higher possibility for the absorption of targeted pollutant molecules during photocatalysis [139,141]. For example, recently research has been done to incorporate noble metals into metal oxides to increase the photocatalytic efficiency of titania [142].

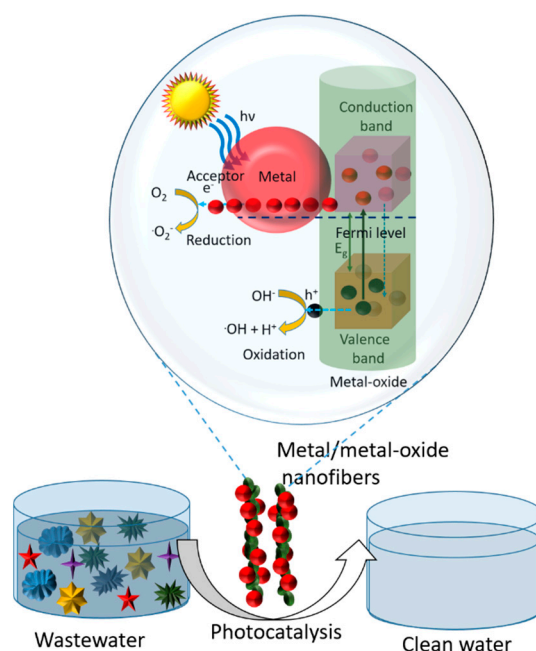


Figure 10. Scheme diagram of the electron transfer mechanism of the metal–metal oxide nanofibers.

Plasmonic properties for the degradation of organic compounds under visible light were first proved by Ohtani's group in 2009 [143] (and even earlier by Tatsuma [144], but for other applications—photocurrent). TiO_2 nanofibers codecorated with Au and Pt nanoparticles for plasmon-enhanced photocatalytic activities were reported by Zhang et al. [145]. These attractive features of metal–metal oxide photocatalytic nanofibers motivated many researchers to investigate the impact of metal nanoparticles on semiconductors during photocatalysis.

7.3. Mechanisms of Photocatalysis by Metal Oxide/Metal Oxide Composite Nanofibers

Coupling metal oxides with other metal oxide semiconductors is another widely held method to tune the optical energy band configuration of photocatalysts and increase photon quantum efficiency, since coupled semiconductors can increase the separation rate of photoinduced electron-hole pairs in photocatalysts. Different from usual semiconductors, metal oxide nanofibers have no forbidden energy gap separating occupied and unoccupied levels, but they can excite electrons between bands to generate a high carrier mobility to simplify kinetic charge separation process. As illustrated in Figure 11, well contacted metal oxide–metal oxide nanofibers are advantageous for forming phase junctions. Generally, in metal/metal oxide semiconductor nanofibers, the metal component can trap the photogenerated charge carriers and promotes the interfacial charge-transfer processes, causing quick recombination and therefore hindering photocatalytic efficiency. In recent years, substantial effort has been employed toward combining metal oxide semiconductor nanostructures with suitable metallic oxide materials to synergize their properties [146–149]. For instance, a metallic metal oxide (Ti_5O_9)–metal oxide (TiO_2) nanocomposite has been developed as the heterojunction to enhance visible-light photocatalytic activity [150]. Compared to the nanoparticles' nanostructures, the TiO_2/ZnO hybrid nanofiber composites are confirmed as a highly efficient photocatalyst for encouraging applications in the wastewater treatment of organic-polluted water [151].

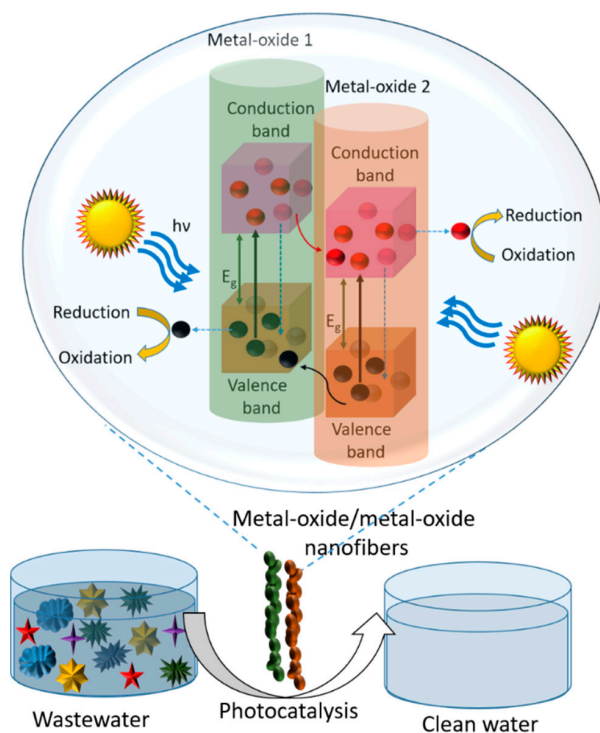


Figure 11. Illustration of charge transfer across the metal oxide–metal oxide nanofiber phase junction and photocatalysis of pollutants.

8. Environmental Remediation Application of Metal Oxide Nanofibers

8.1. Wastewater Treatment

The AOP is a well-known photocatalytic water treatment technique to treat pollutant-containing wastewater, air and various industry effluents and is regarded as one of the most promising methods [152,153]. Figure 12 illustrates how photocatalysis helps degrade organic pollutants in wastewater with the help of metal oxide nanofibers. Common solid metal oxide nanofiber photocatalysts such as TiO_2 , ZnO , WO_3 , and BiVO_4 are known to have outstanding photocatalytic properties. Among them, TiO_2 and ZnO are the most extensively used due to their superior chemical stability, low toxicity, low cost, and extraordinary photocatalytic activity [154,155].

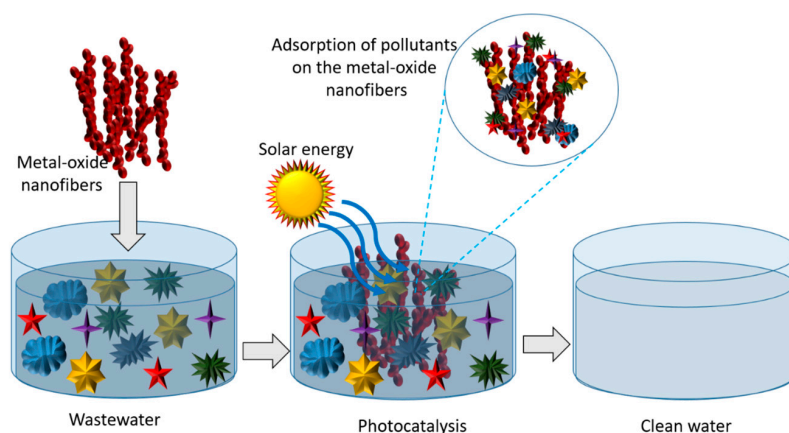


Figure 12. Schematic representation of adsorption and photocatalysis of different kinds of pollutants on metal oxide nanofibers.

Recently, ultrafine porous TiO₂ nanofiber diameters in the range of 10 nm were produced from electrospun rice-shaped TiO₂ nanostructures [156]. The rice-shaped TiO₂ achieved by heating the as-spun TiO₂-polyvinyl acetate composite nanofibers in air followed hydrothermal treatment, acid treatment, and low-temperature sintering. The synthesized TiO₂ nanofibers exhibited better photocatalytic activity than the commercial P-25 TiO₂ towards the degradation of methyl orange dye. ZnO nanofibers are also gaining huge attention in wastewater treatment owing to their outstanding photocatalytic properties; for example, Gupta et al. [157] fabricated photocatalytic ZnO nanofibers by the electrospinning method to degrade acid fuchsin dye in natural solar radiations. A review article on electrospun ZnO nanofibers for the photocatalysis of organic-dye-containing wastewater appeared two years ago from Panthi et al. [158]. Due to their great photocatalytic degradation ability, stable physical properties, low cost, reusability, and recyclability, WO₃ nanofibers have also been studied widely in wastewater treatment [159,160]. Early this year, Ma and coworkers constructed novel WO₃/Fe(III) photocatalytic nanofibers that show enhanced photocatalytic activity by means of interfacial charge transfer effect under visible light irradiation [161]. Furthermore, Bi and its oxides are well-known, cost-effective and multifunctional nanostructured materials, and have attracted numerous interest because of their excellent photocatalytic activity [162,163]. In light to this, bismuth vanadate and cerium dioxide (BiVO₄/CeO₂) composite nanofibers were produced by electrospinning and a homogeneous precipitation method with hydrothermal techniques [164]. Their visible-light-driven photocatalysis was evaluated via the degradation of methylene blue, methyl orange, and a mixture of those dyes. Moreover, a series of environmental remediation applications using metal-metal oxide core-shell nanofibrous nanostructures exploited the special advantages of morphology and highly accessible surface areas [165,166]. One-dimensional magnetite/manganese Fe₂O₃ modified by carbon coating and with TiO₂ nanoparticles into porous core-shell composite nanofibers were fabricated via organometallic compounds as templates [167]. These recyclable metal oxide photocatalytic nanofibers showed superior adsorption and photocatalytic properties for the efficient treatment of aqueous dye-containing waste.

8.2. Water Disinfection and Air Cleansing

The photocatalytic cleaning of wastewater using metal oxide nanocatalysts has attracted substantial research interest over the past few decades. Several types of photocatalysts have been tested for a variety of cleaning applications—for instance, bacterial pollutant and air contaminant removal with wastewater treatment and metal oxide nanofibers [168]. The decontamination of microorganisms from wastewater is an essential application of photocatalysis. The photocatalysts for environmental cleansing applications mostly involve either titanium dioxide or zinc oxide; however, they displayed different activities when they reacted with different bacterial systems. Figure 13 explains the mechanisms for microorganism cleansing using photocatalysis. Photocatalysis is often achieved by damaging the membrane of the bacterial cell and inducing oxidative stress by a highly energetic OH• radical, which is also known as a reactive oxygen species (ROS). This photocatalyst can also attack the bacterial cell wall and release metal ions when needed. For example, a zinc oxide nanofiber can produce zinc ions and a titanium dioxide nanofiber can release titanium. These mechanisms could be more effective when exposed to light illumination. The formation of reactive oxygen species would be significantly greater upon light exposure with photon energy greater than the bandgap energy of the metal oxide nanofiber. However, few metal oxide nanofibers can yield ROS in the absence of photon energy, even upon sub-bandgap radiation.

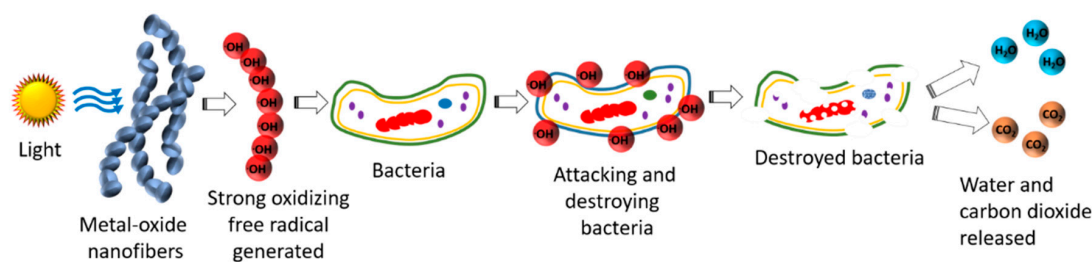


Figure 13. An illustration explaining bacterial disinfection mechanism by nanofiber photocatalyst under light illumination.

The interaction between the nanofibers and bacterial cells could be significantly affected due to the entrapment of photo-generated charge carriers on the surface of the photocatalyst if there is any photocorrosion present. This could change the electrostatic attraction to negatively-charged bacterial cell walls since metal ion release from the metal oxide is heavily affected by photocorrosion.

It is desirable to achieve the bacterial disinfection of wastewater under solar or visible light by nanofiber photocatalysts. While ZnO shows strong antibacterial properties under ambient radiation, TiO₂ generally responds under UV radiation [169,170]. Methods for completing the photocatalysis of waterborne microorganisms into visible and solar light energy have been obtained by making composites, design of core-shell type nanostructures, nanoparticle doping, surface wettability patterning, offset printing, or increase of crystal defect [170].

Photocatalytic disinfection of wastewater using a TiO₂-Pt nanocatalyst was first reported by Matsunaga et al. [171]; they showed the degradation of many microorganisms such as *Lactobacillus acidophilus* (bacteria), *Escherichia coli* (bacteria), and *Saccharomyces cerevisiae* (yeast). It was also confirmed that the catalysts have no toxicity towards human cervical cancer cells (HeLa cells) and photocatalysts could be easily recycled and reused for their antibacterial activities. Last year La₂O₃ nanoparticle-doped PAN nanofiber mats were prepared by an electrospinning process [172]. The metal oxide nanofibers were applied for bacterial inactivation based on a feasible antibacterial strategy through phosphate starvation. In addition to this, the polymer/metal oxide composite nanofiber mats were reusable and easy to recycle.

Above and beyond pollutant and microorganism removal from wastewater, metal oxide nanofibers are also effective in the degradation of volatile organic compounds (VOC), nitrogen oxides, ammonia, sulfur oxides, and carbon monoxide, which are also treated as environmental pollutants [168,173–175].

8.3. Other Applications

Nanofiber nanostructures are also widely involved in several other applications such as textiles, wound dressings, prosthetic kits, dental care, bioimplants, microsurgical and external corporeal devices, drug delivery, tissue engineering, etc. [67,176–178]. In addition, metal oxide nanofibers have revealed a wide spectrum of new applications in energy storage, stem cell research, biomaterial sciences, and biochemistry owing to their favorable morphology and ideal physicochemical properties [104,179–181]. It is worth mentioning that Sabba et al. [182] demonstrated a maskless synthesis of TiO₂-nanofiber-based hierarchical structures and used them in solid-state dye-sensitized solar cells. Volatile organic compound-based sensors have been constructed on electrospun crystalline ZnO and CeO₂/ZnO nanofibrous mats and their sensing characteristics have been demonstrated for benzene, propanol, ethanol, and dichloromethane [183]. Metal oxide nanofibers have found application in tissue engineering, where they could be used as a scaffold material that drives cell differentiation and can create an osteogenic environment without the use of exogenous factors [184]. Carbon-cobalt [185] and highly porous ZnCo₂O₄ composite [186] nanofibers were synthesized by the electrospinning technique and exhibit potential application as an anode material for lithium

ion batteries. Recently, Ali et al. [187] fabricated a microfluidic immuno-biochip to detect breast cancer biomarkers that is based on a hierarchical composite of porous graphene and electrospun TiO_2 nanofibers. Direct electrospinning of titania nanofibers on a conducting electrode was used to construct a cholesterol biosensor (Figure 14 describes the synthesis and application of nanofibers as an enzymatic biosensor) that can detect esterified cholesterol from human blood with excellent sensitivity ($181.6 \mu\text{A}/\text{mg}\cdot\text{dL}^{-1}/\text{cm}^2$) and rapid detection (20 s) [105]. Additionally, metal oxide nanofibers have found huge importance in immunolabeling, cell and molecular bioimaging, biosensing, treatment of tumor cells, soil nutrient sensing, and numerous photosensitive applications [188–192].

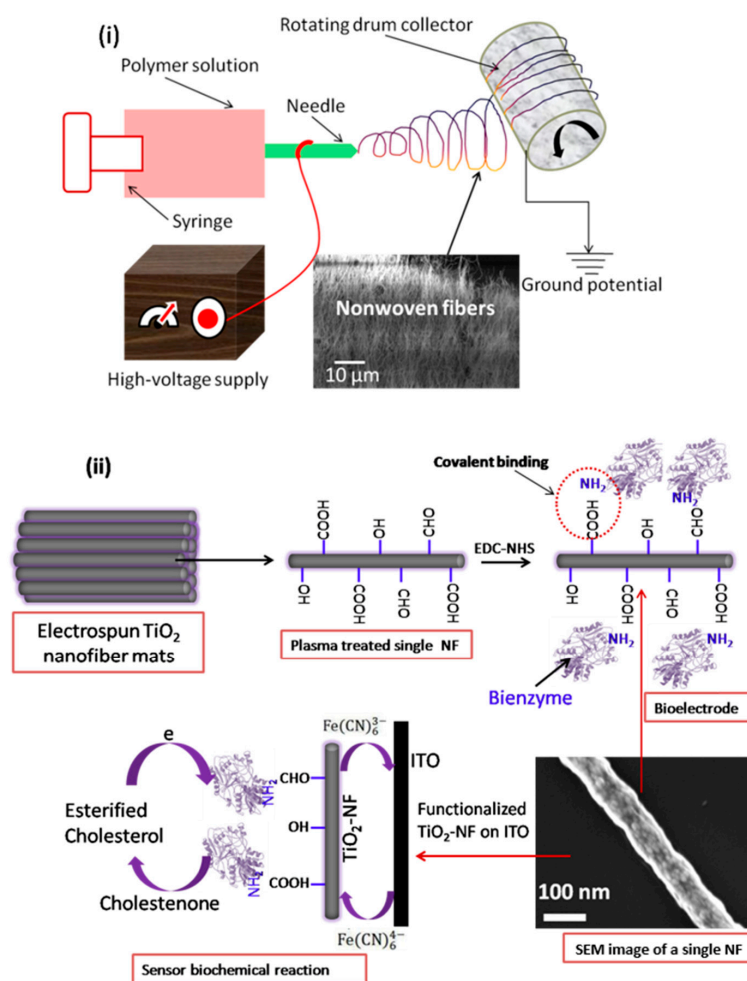


Figure 14. (i) Schematic illustration of the synthesis of TiO_2 nanofibers and (ii) biofunctionalized mesoporous TiO_2 nanofibers for esterified cholesterol detection. Reprinted with permission from [105]. Copyright (2014) American Chemical Society.

9. Recycling of Nanofiber Photocatalysts

While designing a photocatalytic reactor for wastewater treatment, the combination of a high surface area porous catalytic supporter with suitably planned nanostructured photocatalysts together with their recycling and reuse is a must. There are several types of photoreactors that have been used for wastewater treatment such as cascade photoreactor, downflow contactor reactor, and annular slurry reactor. Photocatalytic reactors for wastewater treatment are of two types, depending on the installed state of the photocatalysts, namely slurry reactors with suspended photocatalysts (Figure 15a) and immobilized reactors with photocatalysts immobilized onto a static inert support (Figure 15b). The difference between these two main candidates is that the former needs an extra downstream

separation unit for the recycling and recovery catalysts, whereas the latter permits continuous operation. There is another notable reactor named a tubular continuous flow reactor (shown in Figure 15c). A mechanical peristaltic pump is located between the reactor feed line and the reservoir tank and pumps the polluted water from the main wastewater reservoir to the tubular reaction zone. The reactor tube is of quartz glass coated with nanofiber photocatalysts and designed in such a way that it could harvest a sufficient amount of illuminated light energy for photocatalysis.

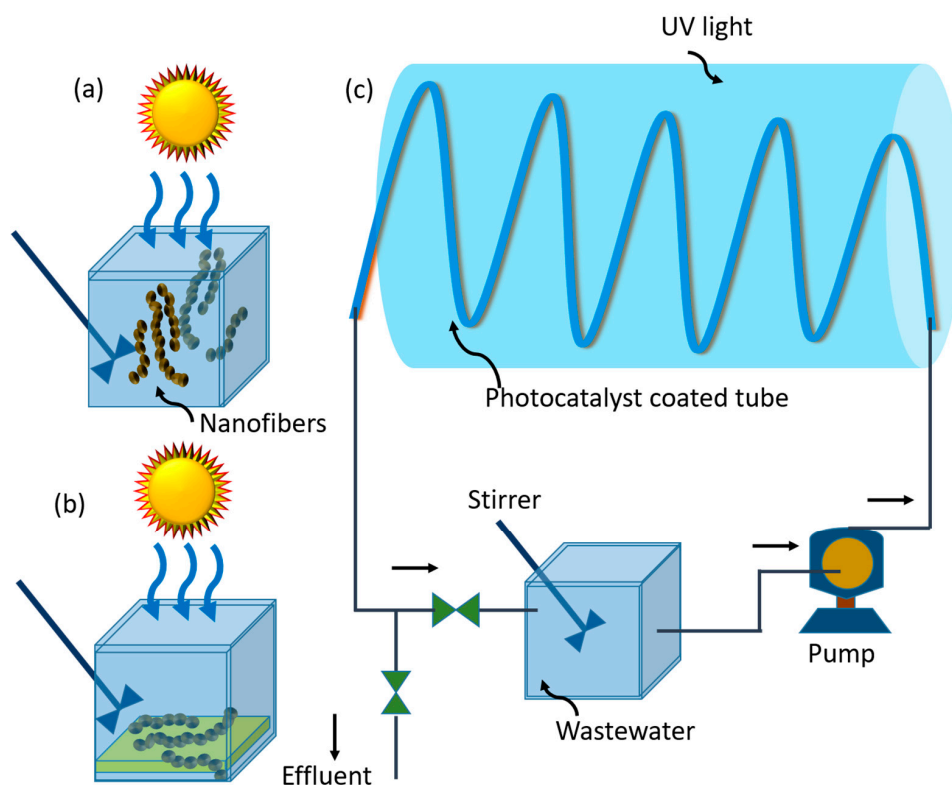


Figure 15. Different types of photocatalytic reactor arrangements: (a) slurry reactor; (b) immobilized reactor; and (c) continuous tubular flow reactor.

The reuse and recycling of photocatalysts is essential since this can reduce the cost of the overall waste management process. Thus, effective engineering is important for creating photocatalysts that could be easily recycled and reused several times. In this context, membrane filtration is a clever exercise for recycling soluble photocatalysts as well. Ultrafiltration and nanofiltration are two familiar membrane filtration techniques for recycling photocatalysts owing to their potential use in enzymatic, organic, and homogeneous catalysis-mediated process intensification at the laboratory level as well as on a larger industrial scale [193,194]. Nanofiltration in continuous flow mode is one more excellent way of recycling nanofiber photocatalysts; however, combining continuous flow with a membrane filtration reactor can be more convenient for efficient wastewater treatment [195]. In this context of recycling, magnetic nanofiber photocatalysts are very useful since they can be easily recycled with an external magnetic field. For example, Zhang et al. [196] synthesized magnetic BiFeO_3 nanofibers with wave node-like morphology by electrospinning. Those nanofibers exhibit highly enhanced photocatalytic properties under visible light. In a recent report, the doping of Fe into a $\text{TiO}_2/\text{SnO}_2$ hybrid nanofiber has also been proven to be an exceptional visible-light-driven photocatalyst with much higher photocatalytic activity than pristine $\text{TiO}_2/\text{SnO}_2$ hybrid nanofibers [197]. The magnetic property against Fe-loading was characterized, and the corresponding photocatalytic activity under visible light was assessed using Rhodamine B degradation as a model pollutant.

Moreover, these nanostructured photocatalytic nanofibers have strong and active magnetic behavior, which makes their recycling and reuse easy. Santala's report suggested a direction for the recycling and recovery of electrospun composite magnetic nanofiber photocatalysts using an external magnetic field [198]. A recycling arrangement based on exchangeable water would be very efficient. Photocatalysis in organic, aqueous, and organic/aqueous media permits easy recovery of homogeneous catalyst nanofibers from the product phase.

10. Conclusions

After reviewing hundreds of the latest representative studies on the role of various semiconductor photocatalysts and their synthesis and applications for environmental remediation, we observed that there are many types of metal oxide photocatalysts nanostructures available depending on the choice of fabrication route and the nature of the application. Among them, metal oxide nanofiber morphologies are reasonably stable and could preserve their structural robustness when reused in an aqueous medium towards environmental remediation, bacterial decontamination, and air purification via ultraviolet, visible, or solar light-driven photocatalysis. Electrospinning has been recognized as an efficient technique for the fabrication of metal oxide nanofibers. Various polymers along with their compatible metal oxide precursors have been successfully electrospun into ultrafine fibers in recent times.

It was shown that photocatalytic oxidation using metal oxide semiconductor photocatalysts has significantly improved the ability to degrade organic pollutants under ultraviolet light. The main problem with photocatalytic AOPs lies in the high cost of reagents such as hydrogen peroxide or energy sources such as ultraviolet light and the higher bandgap energy of several semiconductors. For the photocatalytic oxidation process, the energy demand and cost of the metal oxide/UV could be considerably reduced by the use of solar irradiation and superior nanomorphology to access a higher active surface area. Adjusting their electronic, optical, and physicochemical properties can ensure that the metal oxides efficiently degrade pollutant dyes in visible solar radiation.

The synergistic effect, as depicted in Table 1, indicated the advantages of the application of the photocatalytic oxidation process. Photocatalytic oxidation could be proven as an efficient alternative method for the oxidation and elimination of recalcitrant organic species under specific conditions for the management of agricultural and industrial pollutants in wastewater.

Acknowledgments: Kunal Mondal wants to acknowledge Ashutosh Sharma (Secretary, Department of Science & Technology, New Delhi, India (2015–)), who has inspired many generations of colloid and surface scientists and engineers.

Conflicts of Interest: The authors declare no conflict of interest.

References

1. Kim, S.; Oh, K.; Lee, S.; Choi, S.; Lee, K. Study on secondary reaction and fate of hazardous chemicals by oxidants. *Water Sci. Technol.* **1997**, *36*, 325–331. [[CrossRef](#)]
2. Echigo, S.; Yamada, H.; Matsui, S.; Kawanishi, S.; Shishida, K. Comparison between O₃/VUV, O₃/H₂O₂, VUV and O₃ processes for the decomposition of organophosphoric acid triesters. *Water Sci. Technol.* **1996**, *34*, 81–88. [[CrossRef](#)]
3. Vorontsov, A.V.; Dubovitskaya, V.P. Selectivity of photocatalytic oxidation of gaseous ethanol over pure and modified TiO₂. *J. Catal.* **2004**, *221*, 102–109. [[CrossRef](#)]
4. Hakki, A.; Dillert, R.; Bahnemann, D.W. Factors affecting the selectivity of the photocatalytic conversion of nitroaromatic compounds over TiO₂ to valuable nitrogen-containing organic compounds. *Phys. Chem. Chem. Phys.* **2013**, *15*, 2992–3002. [[CrossRef](#)] [[PubMed](#)]
5. Hu, J.Y.; Wang, Z.S.; Ng, W.J.; Ong, S.L. The effect of water treatment processes on the biological stability of potable water. *Water Res.* **1999**, *33*, 2587–2592. [[CrossRef](#)]
6. Suri, R.P.S.; Liu, J.; Hand, D.W.; Crittenden, J.C.; Perram, D.L.; Mullins, M.E. Heterogeneous photocatalytic oxidation of hazardous organic contaminants in water. *Water Environ. Res.* **1993**, *65*, 665–673. [[CrossRef](#)]

7. Liu, R.; Wang, P.; Wang, X.; Yu, H.; Yu, J. UV- and Visible-Light Photocatalytic Activity of Simultaneously Deposited and Doped Ag/Ag(I)-TiO₂ Photocatalyst. *J. Phys. Chem. C* **2012**, *116*, 17721–17728. [[CrossRef](#)]
8. Kanakaraju, D.; Glass, B.D.; Oelgemöller, M. Titanium dioxide photocatalysis for pharmaceutical wastewater treatment. *Environ. Chem. Lett.* **2014**, *12*, 27–47. [[CrossRef](#)]
9. Chong, M.N.; Jin, B.; Chow, C.W.K.; Saint, C. Recent developments in photocatalytic water treatment technology: A review. *Water Res.* **2010**, *44*, 2997–3027. [[CrossRef](#)] [[PubMed](#)]
10. Pincella, F.; Isozaki, K.; Miki, K. A visible light-driven plasmonic photocatalyst. *Light Sci. Appl.* **2014**, *3*, e133. [[CrossRef](#)]
11. Anjum, M.; Miandad, R.; Waqas, M.; Gehany, F.; Barakat, M.A. Remediation of wastewater using various nano-materials. *Arab. J. Chem.* **2016**. [[CrossRef](#)]
12. Sugunan, A.; Guduru, V.K.; Uheida, A.; Toprak, M.S.; Muhammed, M. Radially Oriented ZnO Nanowires on Flexible Poly-L-Lactide Nanofibers for Continuous-Flow Photocatalytic Water Purification. *J. Am. Ceram. Soc.* **2010**, *93*, 3740–3744. [[CrossRef](#)]
13. Burks, T.; Akthar, F.; Saleemi, M.; Avila, M.; Kiros, Y. ZnO-PLLA Nanofiber Nanocomposite for Continuous Flow Mode Purification of Water from Cr(VI). *J. Environ. Public Health* **2015**, *2015*, 1–7. [[CrossRef](#)] [[PubMed](#)]
14. Singh, P.; Mondal, K.; Sharma, A. Reusable electrospun mesoporous ZnO nanofiber mats for photocatalytic degradation of polycyclic aromatic hydrocarbon dyes in wastewater. *J. Colloid Interface Sci.* **2013**, *394*, 208–215. [[CrossRef](#)] [[PubMed](#)]
15. Mondal, K.; Bhattacharyya, S.; Sharma, A. Photocatalytic Degradation of Naphthalene by Electrospun Mesoporous Carbon-Doped Anatase TiO₂ Nanofiber Mats. *Ind. Eng. Chem. Res.* **2014**, *53*, 18900–18909. [[CrossRef](#)]
16. Hong, H.-J.; Sarkar, S.K.; Lee, B.-T. Formation of TiO₂ nano fibers on a micro-channeled Al₂O₃-ZrO₂/TiO₂ porous composite membrane for photocatalytic filtration. *J. Eur. Ceram. Soc.* **2012**, *32*, 657–663. [[CrossRef](#)]
17. Reddy, K.R.; Gomes, V.G.; Hassan, M. Carbon functionalized TiO₂ nanofibers for high efficiency photocatalysis. *Mater. Res. Express* **2014**, *1*, 015012. [[CrossRef](#)]
18. Singh, N.; Mondal, K.; Misra, M.; Sharma, A.; Gupta, R.K. Quantum dot sensitized electrospun mesoporous titanium dioxide hollow nanofibers for photocatalytic applications. *RSC Adv.* **2016**, *6*, 48109–48119. [[CrossRef](#)]
19. Zhao, D.; He, Z.; Wang, G.; Wang, H.; Zhang, Q.; Li, Y. A novel efficient ZnO/Zn(OH)F nanofiber arrays-based versatile microfluidic system for the applications of photocatalysis and histidine-rich protein separation. *Sens. Actuators B Chem.* **2016**, *229*, 281–287. [[CrossRef](#)]
20. Zhang, L.; Chen, P.; Gu, G.; Wu, Q.; Yao, W. Novel synthesis and photocatalytic performance of Ce_{1-x}Zr_xO₂/silica fiber. *Appl. Surf. Sci.* **2016**, *382*, 155–161. [[CrossRef](#)]
21. Asif, S.A.B.; Khan, S.B.; Asiri, A.M. Visible light functioning photocatalyst based on Al₂O₃ doped Mn₃O₄ nanomaterial for the degradation of organic toxin. *Nanoscale Res. Lett.* **2015**, *10*. [[CrossRef](#)] [[PubMed](#)]
22. Akhi, Y.; Irani, M.; Olya, M.E. Simultaneous degradation of phenol and paracetamol using carbon/MWCNT/Fe₃O₄ composite nanofibers during photo-like-Fenton process. *J. Taiwan Inst. Chem. Eng.* **2016**, *63*, 327–335. [[CrossRef](#)]
23. Wang, J.; Yang, G.; Lyu, W.; Yan, W. Thorny TiO₂ nanofibers: Synthesis, enhanced photocatalytic activity and supercapacitance. *J. Alloys Compd.* **2016**, *659*, 138–145. [[CrossRef](#)]
24. Qin, D.; Lu, W.; Wang, X.; Li, N.; Chen, X.; Zhu, Z.; Chen, W. Graphitic Carbon Nitride from Burial to Re-emergence on Polyethylene Terephthalate Nanofibers as an Easily Recycled Photocatalyst for Degrading Antibiotics under Solar Irradiation. *ACS Appl. Mater. Interfaces* **2016**, *8*, 25962–25970. [[CrossRef](#)] [[PubMed](#)]
25. Wongaree, M.; Chiarakorn, S.; Chuangchote, S.; Sagawa, T. Photocatalytic performance of electrospun CNT/TiO₂ nanofibers in a simulated air purifier under visible light irradiation. *Environ. Sci. Pollut. Res.* **2016**, *23*, 21395–21406. [[CrossRef](#)] [[PubMed](#)]
26. Ma, Z.; Hu, Z.; He, X.; Fang, Z.; Li, Y.; Qiu, J. Nano-Bi₂WO₆ functionalized flexible SiO₂ fibrous film for water purification. *Appl. Surf. Sci.* **2016**, *360*, 174–183. [[CrossRef](#)]
27. Hu, Z.; Ma, Z.; He, X.; Liao, C.; Li, Y.; Qiu, J. Preparation and characterization of flexible and thermally stable CuO nanocrystal-decorated SiO₂ nanofibers. *J. Sol-Gel Sci. Technol.* **2015**, *76*, 492–500. [[CrossRef](#)]
28. Ma, D.; Zhang, Y.; Gao, M.; Xin, Y.; Wu, J.; Bao, N. RGO/InVO₄ hollowed-out nanofibers: Electrospinning synthesis and its application in photocatalysis. *Appl. Surf. Sci.* **2015**, *353*, 118–126. [[CrossRef](#)]

29. Xie, J.; Yang, Y.; He, H.; Cheng, D.; Mao, M.; Jiang, Q.; Song, L.; Xiong, J. Facile synthesis of hierarchical Ag₃PO₄/TiO₂ nanofiber heterostructures with highly enhanced visible light photocatalytic properties. *Appl. Surf. Sci.* **2015**, *355*, 921–929. [[CrossRef](#)]
30. Ofori, F.A.; Sheikh, F.A.; Appiah-Ntiamoah, R.; Yang, X.; Kim, H. A Simple Method of Electrospun Tungsten Trioxide Nanofibers with Enhanced Visible-Light Photocatalytic Activity. *Nano-Micro Lett.* **2015**, *7*, 291–297. [[CrossRef](#)]
31. Zhao, Y.; Tao, C.; Xiao, G.; Wei, G.; Li, L.; Liu, C.; Su, H. Controlled synthesis and photocatalysis of sea urchin-like Fe₃O₄@TiO₂@Ag nanocomposites. *Nanoscale* **2016**, *8*, 5313–5326. [[CrossRef](#)] [[PubMed](#)]
32. Liu, C.; Meng, D.; Li, Y.; Wang, L.; Liu, Y.; Luo, S. Hierarchical architectures of ZnS–In₂S₃ solid solution onto TiO₂ nanofibers with high visible-light photocatalytic activity. *J. Alloys Compd.* **2015**, *624*, 44–52. [[CrossRef](#)]
33. Chen, Y.-Y.; Kuo, C.-C.; Chen, B.-Y.; Chiu, P.-C.; Tsai, P.-C. Multifunctional polyacrylonitrile-ZnO/Ag electrospun nanofiber membranes with various ZnO morphologies for photocatalytic, UV-shielding, and antibacterial applications. *J. Polym. Sci. Part B Polym. Phys.* **2015**, *53*, 262–269. [[CrossRef](#)]
34. Liang, P.; Zhang, L.; Zhao, X.; Li, J.; Liu, L.; Cai, R.; Yang, D.; Umar, A. Synthesis of ZnFe₂O₄/TiO₂ Composite Nanofibers with Enhanced Photoelectrochemical Activity. *Sci. Adv. Mater.* **2015**, *7*, 295–300. [[CrossRef](#)]
35. Zhang, M.; Liu, Y.; Li, L.; Gao, H.; Zhang, X. BiOCl nanosheet/Bi₄Ti₃O₁₂ nanofiber heterostructures with enhanced photocatalytic activity. *Catal. Commun.* **2015**, *58*, 122–126. [[CrossRef](#)]
36. Wang, X.; Gao, J.; Xu, B.; Hua, T.; Xia, H. ZnO nanorod/nickel phthalocyanine hierarchical hetero-nanostructures with superior visible light photocatalytic properties assisted by H₂O₂. *RSC Adv.* **2015**, *5*, 87233–87240. [[CrossRef](#)]
37. Kushwaha, H.S.; Thomas, P.; Vaish, R. Polyaniline/CaCu₃Ti₄O₁₂ nanofiber composite with a synergistic effect on visible light photocatalysis. *RSC Adv.* **2015**, *5*, 87241–87250. [[CrossRef](#)]
38. Galkina, O.L.; Önnéby, K.; Huang, P.; Ivanov, V.K.; Agafonov, A.V.; Seisenbaeva, G.A.; Kessler, V.G. Antibacterial and photochemical properties of cellulose nanofiber–titania nanocomposites loaded with two different types of antibiotic medicines. *J. Mater. Chem. B* **2015**, *3*, 7125–7134. [[CrossRef](#)]
39. Liu, M.; Wang, Y.; Cheng, Z.; Song, L.; Zhang, M.; Hu, M.; Li, J. Function of NaOH hydrolysis in electrospinning ZnO nanofibers via using polylactide as templates. *Mater. Sci. Eng. B* **2014**, *187*, 89–95. [[CrossRef](#)]
40. Kang, H.-J.; Shin, S.-H.; Jo, W.-K.; Chun, H.-H. Visible Light- or UV-Activated Carbon Nanotube-TiO₂ Composite Nanofibers for Indoor BTEX Purification. *Asian J. Chem.* **2014**, *26*. [[CrossRef](#)]
41. Kang, H.-J.; Shin, S.-H.; Chun, H.-H.; Jo, W.-K. Combined Nanofibers of Carbon Nanotube, Titania and Polymer Substrate for Oxidation of Toluene and Isopropyl Alcohol. *Asian J. Chem.* **2014**, *26*. [[CrossRef](#)]
42. Szatmáry, L.; Šubrt, J.; Kalousek, V.; Mosinger, J.; Lang, K. Low-temperature deposition of anatase on nanofiber materials for photocatalytic NO_x removal. *Catal. Today* **2014**, *230*, 74–78. [[CrossRef](#)]
43. Ma, D.; Xin, Y.; Gao, M.; Wu, J. Fabrication and photocatalytic properties of cationic and anionic S-doped TiO₂ nanofibers by electrospinning. *Appl. Catal. B Environ.* **2014**, *147*, 49–57. [[CrossRef](#)]
44. Liu, Z.; Miao, Y.-E.; Liu, M.; Ding, Q.; Tjiu, W.W.; Cui, X.; Liu, T. Flexible polyaniline-coated TiO₂/SiO₂ nanofiber membranes with enhanced visible-light photocatalytic degradation performance. *J. Colloid Interface Sci.* **2014**, *424*, 49–55. [[CrossRef](#)] [[PubMed](#)]
45. Lu, M.; Shao, C.; Wang, K.; Lu, N.; Zhang, X.; Zhang, P.; Zhang, M.; Li, X.; Liu, Y. p-MoO₃ Nanostructures/n-TiO₂ Nanofiber Heterojunctions: Controlled Fabrication and Enhanced Photocatalytic Properties. *ACS Appl. Mater. Interfaces* **2014**, *6*, 9004–9012. [[CrossRef](#)] [[PubMed](#)]
46. Zhang, P.; Shao, C.; Zhang, Z.; Zhang, M.; Mu, J.; Guo, Z.; Sun, Y.; Liu, Y. Core/shell nanofibers of TiO₂@carbon embedded by Ag nanoparticles with enhanced visible photocatalytic activity. *J. Mater. Chem.* **2011**, *21*, 17746. [[CrossRef](#)]
47. Mu, J.; Shao, C.; Guo, Z.; Zhang, Z.; Zhang, M.; Zhang, P.; Chen, B.; Liu, Y. High Photocatalytic Activity of ZnO–Carbon Nanofiber Heteroarchitectures. *ACS Appl. Mater. Interfaces* **2011**, *3*, 590–596. [[CrossRef](#)] [[PubMed](#)]
48. Galland, S.; Andersson, R.L.; Salajková, M.; Ström, V.; Olsson, R.T.; Berglund, L.A. Cellulose nanofibers decorated with magnetic nanoparticles—Synthesis, structure and use in magnetized high toughness membranes for a prototype loudspeaker. *J. Mater. Chem. C* **2013**, *1*, 7963. [[CrossRef](#)]
49. Dzenis, Y. Materials Science: Structural Nanocomposites. *Science* **2008**, *319*, 419–420. [[CrossRef](#)] [[PubMed](#)]

50. Ren, Y.; Wang, S.; Liu, R.; Dai, J.; Liu, X.; Yu, J. A novel route towards well-dispersed short nanofibers and nanoparticles via electrospinning. *RSC Adv.* **2016**, *6*, 30139–30147. [[CrossRef](#)]
51. Tan, E.P.S.; Lim, C.T. Mechanical characterization of nanofibers—A review. *Compos. Sci. Technol.* **2006**, *66*, 1102–1111. [[CrossRef](#)]
52. Zhang, T.; Wu, X.; Luo, T. Polymer Nanofibers with Outstanding Thermal Conductivity and Thermal Stability: Fundamental Linkage between Molecular Characteristics and Macroscopic Thermal Properties. *J. Phys. Chem. C* **2014**, *118*, 21148–21159. [[CrossRef](#)]
53. Lin, T.; Lukas, D.; Bhat, G.S. Nanofiber Manufacture, Properties, and Applications. *J. Nanomater.* **2013**, *2013*, 1. [[CrossRef](#)]
54. Manea, L.R.; Hristian, L.; Leon, A.L.; Popa, A. Recent advances of basic materials to obtain electrospun polymeric nanofibers for medical applications. *IOP Conf. Ser. Mater. Sci. Eng.* **2016**, *145*, 032006. [[CrossRef](#)]
55. Beachley, V.; Wen, X. Effect of electrospinning parameters on the nanofiber diameter and length. *Mater. Sci. Eng. C* **2009**, *29*, 663–668. [[CrossRef](#)] [[PubMed](#)]
56. Nayak, R.; Padhye, R.; Kyratzis, I.L.; Truong, Y.B.; Arnold, L. Recent advances in nanofibre fabrication techniques. *Text. Res. J.* **2011**, *82*, 129–147. [[CrossRef](#)]
57. Moon, S.; Gil, M.; Lee, K.J. Syringeless Electrospinning toward Versatile Fabrication of Nanofiber Web. *Sci. Rep.* **2017**, *7*, 41424. [[CrossRef](#)] [[PubMed](#)]
58. Nakielski, P.; Pawłowska, S.; Pierini, F.; Liwińska, W.; Hejduk, P.; Zembrzycki, K.; Zabost, E.; Kowalewski, T.A. Hydrogel Nanofilaments via Core-Shell Electrospinning. *PLoS ONE* **2015**, *10*, e0129816.
59. Reneker, D.H.; Yarin, A.L. Electrospinning jets and polymer nanofibers. *Polymer* **2008**, *49*, 2387–2425. [[CrossRef](#)]
60. Shao, H.; Ma, Q.; Dong, X.; Yu, W.; Yang, M.; Yang, Y.; Wang, J.; Liu, G. Electrospun Flexible Coaxial Nanoribbons Endowed With Tuned and Simultaneous Fluorescent Color-Electricity-Magnetism Trifunctionality. *Sci. Rep.* **2015**, *5*, 14052. [[CrossRef](#)] [[PubMed](#)]
61. Lin, T.; Wang, H.; Wang, X. Self-Crimping Bicomponent Nanofibers Electrospun from Polyacrylonitrile and Elastomeric Polyurethane. *Adv. Mater.* **2005**, *17*, 2699–2703. [[CrossRef](#)]
62. De Jong, K.P.; Geus, J.W. Carbon Nanofibers: Catalytic Synthesis and Applications. *Catal. Rev.* **2000**, *42*, 481–510. [[CrossRef](#)]
63. Mirjalili, M.; Zohoori, S. Review for application of electrospinning and electrospun nanofibers technology in textile industry. *J. Nanostruct. Chem.* **2016**, *6*, 207–213. [[CrossRef](#)]
64. Ding, B.; Wang, M.; Yu, J.; Sun, G. Gas Sensors Based on Electrospun Nanofibers. *Sensors* **2009**, *9*, 1609–1624. [[CrossRef](#)] [[PubMed](#)]
65. Thavasi, V.; Singh, G.; Ramakrishna, S. Electrospun nanofibers in energy and environmental applications. *Energy Environ. Sci.* **2008**, *1*, 205. [[CrossRef](#)]
66. Daniele, M.A.; Boyd, D.A.; Adams, A.A.; Ligler, F.S. Microfluidic Strategies for Design and Assembly of Microfibers and Nanofibers with Tissue Engineering and Regenerative Medicine Applications. *Adv. Healthc. Mater.* **2015**, *4*, 11–28. [[CrossRef](#)] [[PubMed](#)]
67. Teo, W.E.; Ramakrishna, S. A review on electrospinning design and nanofibre assemblies. *Nanotechnology* **2006**, *17*, R89. [[CrossRef](#)] [[PubMed](#)]
68. Murugan, R.; Ramakrishna, S. Nano-Featured Scaffolds for Tissue Engineering: A Review of Spinning Methodologies. *Tissue Eng.* **2006**, *12*, 435–447. [[CrossRef](#)] [[PubMed](#)]
69. Khajavi, R.; Abbasipour, M. Electrospinning as a versatile method for fabricating coreshell, hollow and porous nanofibers. *Sci. Iran.* **2012**, *19*, 2029–2034. [[CrossRef](#)]
70. Reneker, D.H.; Chun, I. Nanometre diameter fibres of polymer, produced by electrospinning. *Nanotechnology* **1996**, *7*, 216. [[CrossRef](#)]
71. Zhou, Y.; Freitag, M.; Hone, J.; Staii, C.; Johnson, A.T.; Pinto, N.J.; MacDiarmid, A.G. Fabrication and electrical characterization of polyaniline-based nanofibers with diameter below 30 nm. *Appl. Phys. Lett.* **2003**, *83*, 3800–3802. [[CrossRef](#)]
72. Pillay, V.; Dott, C.; Choonara, Y.E.; Tyagi, C.; Tomar, L.; Kumar, P.; du Toit, L.C.; Ndesendo, V.M.K. A Review of the Effect of Processing Variables on the Fabrication of Electrospun Nanofibers for Drug Delivery Applications. *J. Nanomater.* **2013**, *2013*, 1–22. [[CrossRef](#)]

73. Bae, H.-S.; Haider, A.; Selim, K.M.K.; Kang, D.-Y.; Kim, E.-J.; Kang, I.-K. Fabrication of highly porous PMMA electrospun fibers and their application in the removal of phenol and iodine. *J. Polym. Res.* **2013**, *20*. [[CrossRef](#)]
74. Haider, S.; Al-Zeghayer, Y.; Ahmed Ali, F.A.; Haider, A.; Mahmood, A.; Al-Masry, W.A.; Imran, M.; Aijaz, M.O. Highly aligned narrow diameter chitosan electrospun nanofibers. *J. Polym. Res.* **2013**, *20*. [[CrossRef](#)]
75. Sun, Z.; Zussman, E.; Yarin, A.L.; Wendorff, J.H.; Greiner, A. Compound Core–Shell Polymer Nanofibers by Co-Electrospinning. *Adv. Mater.* **2003**, *15*, 1929–1932. [[CrossRef](#)]
76. Elahi, M.F.; Lu, W. Core-shell Fibers for Biomedical Applications—A Review. *J. Bioeng. Biomed. Sci.* **2013**, *3*. [[CrossRef](#)]
77. Yarin, A.L.; Zussman, E.; Wendorff, J.H.; Greiner, A. Material encapsulation and transport in core–shell micro/nanofibers, polymer and carbon nanotubes and micro/nanochannels. *J. Mater. Chem.* **2007**, *17*, 2585–2599. [[CrossRef](#)]
78. Agarwal, S.; Wendorff, J.H.; Greiner, A. Use of electrospinning technique for biomedical applications. *Polymer* **2008**, *49*, 5603–5621. [[CrossRef](#)]
79. Li, D.; Xia, Y. Electrospinning of Nanofibers: Reinventing the Wheel? *Adv. Mater.* **2004**, *16*, 1151–1170. [[CrossRef](#)]
80. Dalton, P.D.; Klee, D.; Möller, M. Electrospinning with dual collection rings. *Polymer* **2005**, *46*, 611–614. [[CrossRef](#)]
81. Hou, H.; Jun, Z.; Reuning, A.; Schaper, A.; Wendorff, J.H.; Greiner, A. Poly(*p*-xylylene) Nanotubes by Coating and Removal of Ultrathin Polymer Template Fibers. *Macromolecules* **2002**, *35*, 2429–2431. [[CrossRef](#)]
82. Bognitzki, M.; Frese, T.; Steinhart, M.; Greiner, A.; Wendorff, J.H.; Schaper, A.; Hellwig, M. Preparation of fibers with nanoscaled morphologies: Electrospinning of polymer blends. *Polym. Eng. Sci.* **2001**, *41*, 982–989. [[CrossRef](#)]
83. Zhan, S.; Chen, D.; Jiao, X.; Tao, C. Long TiO₂ Hollow Fibers with Mesoporous Walls: Sol–Gel Combined Electrospun Fabrication and Photocatalytic Properties. *J. Phys. Chem. B* **2006**, *110*, 11199–11204. [[CrossRef](#)] [[PubMed](#)]
84. Zhan, S.; Chen, D.; Jiao, X.; Liu, S. Facile fabrication of long α -Fe₂O₃, α -Fe and γ -Fe₂O₃ hollow fibers using sol–gel combined co-electrospinning technology. *J. Colloid Interface Sci.* **2007**, *308*, 265–270. [[CrossRef](#)] [[PubMed](#)]
85. Gu, Y.; Jian, F. Hollow LiNi_{0.8}Co_{0.1}Mn_{0.1}O₂–MgO Coaxial Fibers: Sol–Gel Method Combined with Co-electrospun Preparation and Electrochemical Properties. *J. Phys. Chem. C* **2008**, *112*, 20176–20180. [[CrossRef](#)]
86. Rahmathullah, A.M.; Jason Robinette, E.; Chen, H.; Elabd, Y.A.; Palmese, G.R. Plasma assisted synthesis of hollow nanofibers using electrospun sacrificial templates. *Nucl. Instrum. Methods Phys. Res. Sect. B* **2007**, *265*, 23–30. [[CrossRef](#)]
87. Ge, L.; Pan, C.; Chen, H.; Wang, X.; Wang, C.; Gu, Z. The fabrication of hollow multilayered polyelectrolyte fibrous mats and its morphology study. *Colloids Surf. Physicochem. Eng. Asp.* **2007**, *293*, 272–277. [[CrossRef](#)]
88. Zhang, T.; Ge, L.; Wang, X.; Gu, Z. Hollow TiO₂ containing multilayer nanofibers with enhanced photocatalytic activity. *Polymer* **2008**, *49*, 2898–2902. [[CrossRef](#)]
89. Cui, Q.; Dong, X.; Wang, J.; Li, M. Direct fabrication of cerium oxide hollow nanofibers by electrospinning. *J. Rare Earths* **2008**, *26*, 664–669. [[CrossRef](#)]
90. Meng, B.; Tan, X.; Meng, X.; Qiao, S.; Liu, S. Porous and dense Ni hollow fibre membranes. *J. Alloys Compd.* **2009**, *470*, 461–464. [[CrossRef](#)]
91. Sundarajan, S.; Tan, K.L.; Lim, S.H.; Ramakrishna, S. Electrospun Nanofibers for Air Filtration Applications. *Procedia Eng.* **2014**, *75*, 159–163. [[CrossRef](#)]
92. Zainoodin, A.M.; Kamarudin, S.K.; Masdar, M.S.; Daud, W.R.W.; Mohamad, A.B.; Sahari, J. High power direct methanol fuel cell with a porous carbon nanofiber anode layer. *Appl. Energy* **2014**, *113*, 946–954. [[CrossRef](#)]
93. Patel, A.C.; Li, S.; Wang, C.; Zhang, W.; Wei, Y. Electrospinning of Porous Silica Nanofibers Containing Silver Nanoparticles for Catalytic Applications. *Chem. Mater.* **2007**, *19*, 1231–1238. [[CrossRef](#)]
94. Smith, I.O.; Liu, X.H.; Smith, L.A.; Ma, P.X. Nanostructured polymer scaffolds for tissue engineering and regenerative medicine. *Wiley Interdiscip. Rev. Nanomed. Nanobiotechnol.* **2009**, *1*, 226–236. [[CrossRef](#)] [[PubMed](#)]

95. Loh, Q.L.; Choong, C. Three-Dimensional Scaffolds for Tissue Engineering Applications: Role of Porosity and Pore Size. *Tissue Eng. Part B Rev.* **2013**, *19*, 485–502. [[CrossRef](#)] [[PubMed](#)]
96. Chou, S.-F.; Carson, D.; Woodrow, K.A. Current strategies for sustaining drug release from electrospun nanofibers. *J. Controlled Release* **2015**, *220*, 584–591. [[CrossRef](#)] [[PubMed](#)]
97. Mondal, K.; Ali, M.A.; Singh, C.; Sumana, G.; Malhotra, B.D.; Sharma, A. Highly sensitive porous carbon and metal/carbon conducting nanofiber based enzymatic biosensors for triglyceride detection. *Sens. Actuators B Chem.* **2017**, *246*, 202–214. [[CrossRef](#)]
98. Chung, H.J.; Park, T.G. Surface engineered and drug releasing pre-fabricated scaffolds for tissue engineering. *Matrices Scaffolds Drug Deliv. Tissue Eng.* **2007**, *59*, 249–262. [[CrossRef](#)] [[PubMed](#)]
99. Nayani, K.; Katepalli, H.; Sharma, C.S.; Sharma, A.; Patil, S.; Venkataraghavan, R. Electrospinning Combined with Nonsolvent-Induced Phase Separation To Fabricate Highly Porous and Hollow Submicrometer Polymer Fibers. *Ind. Eng. Chem. Res.* **2012**, *51*, 1761–1766. [[CrossRef](#)]
100. Ramakrishna, S. *An Introduction to Electrospinning and Nanofibers*; World Scientific: Singapore; Hackensack, NJ, USA, 2005.
101. Barhate, R.; Ramakrishna, S. Nanofibrous filtering media: Filtration problems and solutions from tiny materials. *J. Membr. Sci.* **2007**, *296*, 1–8. [[CrossRef](#)]
102. Peng, M.; Li, D.; Shen, L.; Chen, Y.; Zheng, Q.; Wang, H. Nanoporous Structured Submicrometer Carbon Fibers Prepared via Solution Electrospinning of Polymer Blends. *Langmuir* **2006**, *22*, 9368–9374. [[CrossRef](#)] [[PubMed](#)]
103. Qi, Z.; Yu, H.; Chen, Y.; Zhu, M. Highly porous fibers prepared by electrospinning a ternary system of nonsolvent/solvent/poly(L-lactic acid). *Mater. Lett.* **2009**, *63*, 415–418. [[CrossRef](#)]
104. Mondal, K.; Sharma, A. Recent advances in electrospun metal-oxide nanofiber based interfaces for electrochemical biosensing. *RSC Adv.* **2016**, *6*, 94595–94616. [[CrossRef](#)]
105. Mondal, K.; Ali, M.A.; Agrawal, V.V.; Malhotra, B.D.; Sharma, A. Highly Sensitive Biofunctionalized Mesoporous Electrospun TiO₂ Nanofiber Based Interface for Biosensing. *ACS Appl. Mater. Interfaces* **2014**, *6*, 2516–2527. [[CrossRef](#)] [[PubMed](#)]
106. Ali, M.A.; Mondal, K.; Singh, C.; Dhar Malhotra, B.; Sharma, A. Anti-epidermal growth factor receptor conjugated mesoporous zinc oxide nanofibers for breast cancer diagnostics. *Nanoscale* **2015**, *7*, 7234–7245. [[CrossRef](#)] [[PubMed](#)]
107. Park, S.-H.; Jung, H.-R.; Lee, W.-J. Hollow activated carbon nanofibers prepared by electrospinning as counter electrodes for dye-sensitized solar cells. *Electrochimica Acta* **2013**, *102*, 423–428. [[CrossRef](#)]
108. Crespy, D.; Friedemann, K.; Popa, A.-M. Colloid-Electrospinning: Fabrication of Multicompartment Nanofibers by the Electrospinning of Organic or/and Inorganic Dispersions and Emulsions. *Macromol. Rapid Commun.* **2012**, *33*, 1978–1995. [[CrossRef](#)] [[PubMed](#)]
109. Shi, X.; Zhou, W.; Ma, D.; Ma, Q.; Bridges, D.; Ma, Y.; Hu, A. Electrospinning of Nanofibers and Their Applications for Energy Devices. *J. Nanomater.* **2015**, *2015*, 1–20. [[CrossRef](#)]
110. Şimşek, M.; Rzayev, Z.M.O.; Bunyatova, U. Multifunctional electroactive electrospun nanofiber structures from water solution blends of PVA/ODA–MMT and poly(maleic acid-*alt*-acrylic acid): Effects of Ag, organoclay, structural rearrangement and NaOH doping factors. *Adv. Nat. Sci. Nanosci. Nanotechnol.* **2016**, *7*, 025009. [[CrossRef](#)]
111. Li, L.; Meyer, W.H.; Wegner, G.; Wohlfahrt-Mehrens, M. Synthesis of Submicrometer-Sized Electrochemically Active Lithium Cobalt Oxide via a Polymer Precursor. *Adv. Mater.* **2005**, *17*, 984–988. [[CrossRef](#)]
112. Lu, G.; Lieberwirth, I.; Wegner, G. A General Polymer-Based Process to Prepare Mixed Metal Oxides: The Case of Zn_{1-x}Mg_xO Nanoparticles. *J. Am. Chem. Soc.* **2006**, *128*, 15445–15450. [[CrossRef](#)] [[PubMed](#)]
113. Qin, D.; Gu, A.; Liang, G.; Yuan, L. A facile method to prepare zirconia electrospun fibers with different morphologies and their novel composites based on cyanate ester resin. *RSC Adv.* **2012**, *2*, 1364–1372. [[CrossRef](#)]
114. Ko, J.-B.; Lee, S.W.; Kim, D.E.; Kim, Y.U.; Li, G.; Lee, S.G.; Chang, T.-S.; Kim, D.; Joo, Y.L. Fabrication of SiO₂-ZrO₂ composite fiber mats via electrospinning. *J. Porous Mater.* **2006**, *13*, 325–330. [[CrossRef](#)]
115. Qin, D.; Liang, G.; Gu, A.; Yuan, L. Fabrication of SiO₂ covered ZrO₂ electrospun fibres with controllable structure and their novel high-performance composites with outstanding thermal, mechanical and dielectric properties. *J. Compos. Mater.* **2014**, *48*, 3201–3214. [[CrossRef](#)]

116. Jiang, Y.; Zhang, Y.; Bai, J.; Ma, Z.; Cui, J. Facile Synthesis via Electrospinning of a Tetraethoxysilane/Polyvinylpyrrolidone Sol and Characterization of Ultrafine Crystalline SiO₂ Nanofibers. *J. Macromol. Sci. Part B* **2014**, *53*, 383–390. [[CrossRef](#)]
117. Chen, Y.; Zhang, Z.; Yu, J.; Guo, Z.-X. Poly(methyl methacrylate)/silica nanocomposite fibers by electrospinning. *J. Polym. Sci. Part B Polym. Phys.* **2009**, *47*, 1211–1218. [[CrossRef](#)]
118. Friedemann, K.; Corrales, T.; Kappl, M.; Landfester, K.; Crespy, D. Facile and Large-Scale Fabrication of Anisometric Particles from Fibers Synthesized by Colloid-Electrospinning. *Small* **2012**, *8*, 144–153. [[CrossRef](#)] [[PubMed](#)]
119. Kanehata, M.; Ding, B.; Shiratori, S. Nanoporous ultra-high specific surface inorganic fibres. *Nanotechnology* **2007**, *18*, 315602. [[CrossRef](#)]
120. Horzum, N.; Taşçıoğlu, D.; Okur, S.; Demir, M.M. Humidity sensing properties of ZnO-based fibers by electrospinning. *Talanta* **2011**, *85*, 1105–1111. [[CrossRef](#)] [[PubMed](#)]
121. Imran, Z.; Rasool, K.; Batool, S.S.; Ahmad, M.; Rafiq, M.A. Effect of different electrodes on the transport properties of ZnO nanofibers under humid environment. *AIP Adv.* **2015**, *5*, 117214. [[CrossRef](#)]
122. Subjalearndee, N.; Intasanta, V. Thermal relaxation in combination with fiberglass confined interpenetrating networks: A key calcination process for as-desired free standing metal oxide nanofibrous membranes. *RSC Adv.* **2016**, *6*, 86798–86807. [[CrossRef](#)]
123. Lim, J.-M.; Moon, J.H.; Yi, G.-R.; Heo, C.-J.; Yang, S.-M. Fabrication of One-Dimensional Colloidal Assemblies from Electrospun Nanofibers. *Langmuir* **2006**, *22*, 3445–3449. [[CrossRef](#)] [[PubMed](#)]
124. Li, D.; Xia, Y. Fabrication of Titania Nanofibers by Electrospinning. *Nano Lett.* **2003**, *3*, 555–560. [[CrossRef](#)]
125. Kim, J.-H.; Yoo, S.-J.; Kwak, D.-H.; Jung, H.-J.; Kim, T.-Y.; Park, K.-H.; Lee, J.-W. Characterization and application of electrospun alumina nanofibers. *Nanoscale Res. Lett.* **2014**, *9*, 44. [[CrossRef](#)] [[PubMed](#)]
126. Calza, P.; Minero, C.; Pelizzetti, E. Photocatalytically Assisted Hydrolysis of Chlorinated Methanes under Anaerobic Conditions. *Environ. Sci. Technol.* **1997**, *31*, 2198–2203. [[CrossRef](#)]
127. Davis, A.P.; Green, D.L. Photocatalytic Oxidation of Cadmium-EDTA with Titanium Dioxide. *Environ. Sci. Technol.* **1999**, *33*, 609–617. [[CrossRef](#)]
128. Schmelling, D.C.; Gray, K.A.; Kamat, P.V. The influence of solution matrix on the photocatalytic degradation of TNT in TiO₂ slurries. *Water Res.* **1997**, *31*, 1439–1447. [[CrossRef](#)]
129. Topalov, A.; Molnár-Gábor, D.; Csanádi, J. Photocatalytic oxidation of the fungicide metalaxyl dissolved in water over TiO₂. *Water Res.* **1999**, *33*, 1371–1376. [[CrossRef](#)]
130. Ku, Y.; Leu, R.-M.; Lee, K.-C. Decomposition of 2-chlorophenol in aqueous solution by UV irradiation with the presence of titanium dioxide. *Water Res.* **1996**, *30*, 2569–2578. [[CrossRef](#)]
131. Serpone, N.; Emeline, A.V. Suggested terms and definitions in photocatalysis and radiocatalysis. *Int. J. Photoenergy* **2002**, *4*, 91–131. [[CrossRef](#)]
132. Agustina, T.E.; Ang, H.M.; Vareek, V.K. A review of synergistic effect of photocatalysis and ozonation on wastewater treatment. *J. Photochem. Photobiol. C Photochem. Rev.* **2005**, *6*, 264–273. [[CrossRef](#)]
133. Legrini, O.; Oliveros, E.; Braun, A.M. Photochemical processes for water treatment. *Chem. Rev.* **1993**, *93*, 671–698. [[CrossRef](#)]
134. Gerischer, H.; Lübke, M. A particle size effect in the sensitization of TiO₂ electrodes by a CdS deposit. *J. Electroanal. Chem. Interfacial Electrochem.* **1986**, *204*, 225–227. [[CrossRef](#)]
135. Bard, A.J.; Fox, M.A. Artificial Photosynthesis: Solar Splitting of Water to Hydrogen and Oxygen. *Acc. Chem. Res.* **1995**, *28*, 141–145. [[CrossRef](#)]
136. Baba, R.; Nakabayashi, S.; Fujishima, A.; Honda, K. Investigation of the mechanism of hydrogen evolution during photocatalytic water decomposition on metal-loaded semiconductor powders. *J. Phys. Chem.* **1985**, *89*, 1902–1905. [[CrossRef](#)]
137. Vinodgopal, K.; Kamat, P.V. Enhanced Rates of Photocatalytic Degradation of an Azo Dye Using SnO₂/TiO₂ Coupled Semiconductor Thin Films. *Environ. Sci. Technol.* **1995**, *29*, 841–845. [[CrossRef](#)] [[PubMed](#)]
138. Jiang, T.; Qin, X.; Sun, Y.; Yu, M. UV photocatalytic activity of Au@ZnO core-shell nanostructure with enhanced UV emission. *RSC Adv.* **2015**, *5*, 65595–65599. [[CrossRef](#)]
139. Costi, R.; Saunders, A.E.; Banin, U. Colloidal hybrid nanostructures: A new type of functional materials. *Angew. Chem. Int. Ed.* **2010**, *49*, 4878–4897. [[CrossRef](#)] [[PubMed](#)]
140. Manninen, H.E.; Flagan, R.C. A new high-transmission inlet for the Caltech nano-RDMA for size distribution measurements of sub-3 nm ions at ambient concentrations. *Atmospheric Meas. Tech.* **2016**, *9*, 2709.

141. Sheldon, M.T.; Trudeau, P.-E.; Mokari, T.; Wang, L.-W.; Alivisatos, A.P. Enhanced semiconductor nanocrystal conductance via solution grown contacts. *Nano Lett.* **2009**, *9*, 3676–3682. [[CrossRef](#)] [[PubMed](#)]
142. Li, H.; Liu, E.; Fan, J.; Hu, X.; Wan, J.; Sun, L.; Hu, Y. Fabrication of plasmonic Au/TiO₂ nanofiber films with enhanced photocatalytic activities. *Appl. Opt.* **2016**, *55*, 221–227. [[CrossRef](#)] [[PubMed](#)]
143. Kowalska, E.; Abe, R.; Ohtani, B. Visible light-induced photocatalytic reaction of gold-modified titanium(IV) oxide particles: Action spectrum analysis. *Chem. Commun.* **2009**, 241–243. [[CrossRef](#)] [[PubMed](#)]
144. Tian, Y.; Tatsuma, T. Mechanisms and Applications of Plasmon-Induced Charge Separation at TiO₂ Films Loaded with Gold Nanoparticles. *J. Am. Chem. Soc.* **2005**, *127*, 7632–7637. [[CrossRef](#)] [[PubMed](#)]
145. Zhang, Z.; Wang, Z.; Cao, S.-W.; Xue, C. Au/Pt Nanoparticle-Decorated TiO₂ Nanofibers with Plasmon-Enhanced Photocatalytic Activities for Solar-to-Fuel Conversion. *J. Phys. Chem. C* **2013**, *117*, 25939–25947. [[CrossRef](#)]
146. Wang, M.; Cui, L.; Li, S.; Li, Z.; Ma, T.; Luan, G.; Liu, W.; Zhang, F. Facile fabrication hybrids of TiO₂@ZnO tubes with enhanced photocatalytic properties. *RSC Adv.* **2016**, *6*, 58452–58457. [[CrossRef](#)]
147. Hou, L.-R.; Yuan, C.-Z.; Peng, Y. Synthesis and photocatalytic property of SnO₂/TiO₂ nanotubes composites. *J. Hazard. Mater.* **2007**, *139*, 310–315. [[CrossRef](#)] [[PubMed](#)]
148. Xu, X.; Yang, G.; Liang, J.; Ding, S.; Tang, C.; Yang, H.; Yan, W.; Yang, G.; Yu, D. Fabrication of one-dimensional heterostructured TiO₂@SnO₂ with enhanced photocatalytic activity. *J. Mater. Chem. A* **2014**, *2*, 116–122. [[CrossRef](#)]
149. Réti, B.; Péter, N.; Dombi, A.; Hernadi, K. Preparation of SnO₂-TiO₂/MWCNT nanocomposite photocatalysts with different synthesis parameters. *Phys. Status Solidi B* **2013**, *250*, 2549–2553. [[CrossRef](#)]
150. Li, L.H.; Deng, Z.X.; Xiao, J.X.; Yang, G.W. A metallic metal oxide (Ti₅O₉)-metal oxide (TiO₂) nanocomposite as the heterojunction to enhance visible-light photocatalytic activity. *Nanotechnology* **2015**, *26*, 255705. [[CrossRef](#)] [[PubMed](#)]
151. Liu, R.; Ye, H.; Xiong, X.; Liu, H. Fabrication of TiO₂/ZnO composite nanofibers by electrospinning and their photocatalytic property. *Mater. Chem. Phys.* **2010**, *121*, 432–439. [[CrossRef](#)]
152. Rauf, M.A.; Ashraf, S.S. Radiation induced degradation of dyes—An overview. *J. Hazard. Mater.* **2009**, *166*, 6–16. [[CrossRef](#)] [[PubMed](#)]
153. Sakkas, V.A.; Islam, M.A.; Stalikas, C.; Albanis, T.A. Photocatalytic degradation using design of experiments: A review and example of the Congo red degradation. *J. Hazard. Mater.* **2010**, *175*, 33–44. [[CrossRef](#)] [[PubMed](#)]
154. Orha, C.; Manea, F.; Pop, A.; Bandas, C.; Lazau, C. TiO₂-nanostructured carbon composite sorbent/photocatalyst for humic acid removal from water. *Desalination Water Treat.* **2016**, *57*, 14178–14187. [[CrossRef](#)]
155. Chan, S.H.S.; Yeong Wu, T.; Juan, J.C.; Teh, C.Y. Recent developments of metal oxide semiconductors as photocatalysts in advanced oxidation processes (AOPs) for treatment of dye waste-water. *J. Chem. Technol. Biotechnol.* **2011**, *86*, 1130–1158. [[CrossRef](#)]
156. Chacko, D.K.; Madhavan, A.A.; Arun, T.A.; Thomas, S.; Anjusree, G.S.; Deepak, T.G.; Balakrishnan, A.; Subramanian, K.R.V.; Sivakumar, N.; Nair, S.V.; et al. Ultrafine TiO₂ nanofibers for photocatalysis. *RSC Adv.* **2013**, *3*, 24858–24862. [[CrossRef](#)]
157. Gupta, A.; Nandanwar, D.V.; Dhakate, S.R. Electrospun Self-assembled ZnO Nanofibers Structures for Photocatalytic Activity in Natural Solar Radiations to Degrade Acid Fuchsin Dye. *Adv. Mater. Lett.* **2015**, *6*, 706–710. [[CrossRef](#)]
158. Panthi, G.; Park, M.; Kim, H.-Y.; Lee, S.-Y.; Park, S.-J. Electrospun ZnO hybrid nanofibers for photodegradation of wastewater containing organic dyes: A review. *J. Ind. Eng. Chem.* **2015**, *21*, 26–35. [[CrossRef](#)]
159. Taha, A.A.; Li, F. Porous WO₃-carbon nanofibers: High-performance and recyclable visible light photocatalysis. *Catal. Sci. Technol.* **2014**, *4*, 3601–3605. [[CrossRef](#)]
160. Chen, Z.; Zhao, J.; Yang, X.; Ye, Q.; Huang, K.; Hou, C.; Zhao, Z.; You, J.; Li, Y. Fabrication of TiO₂/WO₃ Composite Nanofibers by Electrospinning and Photocatalytic Performance of the Resultant Fabrics. *Ind. Eng. Chem. Res.* **2016**, *55*, 80–85. [[CrossRef](#)]
161. Ma, G.; Chen, Z.; Chen, Z.; Jin, M.; Meng, Q.; Yuan, M.; Wang, X.; Liu, J.-M.; Zhou, G. Constructing novel WO₃/Fe(III) nanofibers photocatalysts with enhanced visible-light-driven photocatalytic activity via interfacial charge transfer effect. *Mater. Today Energy* **2017**, *3*, 45–52. [[CrossRef](#)]

162. Liu, G.; Liu, S.; Lu, Q.; Sun, H.; Xiu, Z. Synthesis and characterization of $\text{Bi}(\text{VO}_4)_{1-m}(\text{PO}_4)_m$ nanofibers by electrospinning process with enhanced photocatalytic activity under visible light. *RSC Adv.* **2014**, *4*, 33695–33701. [[CrossRef](#)]
163. Liu, H.; Hou, H.; Gao, F.; Yao, X.; Yang, W. Tailored Fabrication of Thoroughly Mesoporous BiVO_4 Nanofibers and Their Visible-Light Photocatalytic Activities. *ACS Appl. Mater. Interfaces* **2016**, *8*, 1929–1936. [[CrossRef](#)] [[PubMed](#)]
164. Wetchakun, N.; Chaiwichain, S.; Inceesungvorn, B.; Pingmuang, K.; Phanichphant, S.; Minett, A.I.; Chen, J. $\text{BiVO}_4/\text{CeO}_2$ Nanocomposites with High Visible-Light-Induced Photocatalytic Activity. *ACS Appl. Mater. Interfaces* **2012**, *4*, 3718–3723. [[CrossRef](#)] [[PubMed](#)]
165. Misra, M.; Singh, N.; Gupta, R.K. Enhanced visible-light-driven photocatalytic activity of Au@Ag core-shell bimetallic nanoparticles immobilized on electrospun TiO_2 nanofibers for degradation of organic compounds. *Catal. Sci. Technol.* **2017**, *7*, 570–580. [[CrossRef](#)]
166. Hou, H.; Shang, M.; Wang, L.; Li, W.; Tang, B.; Yang, W. Efficient Photocatalytic Activities of TiO_2 Hollow Fibers with Mixed Phases and Mesoporous Walls. *Sci. Rep.* **2015**, *5*, 15228. [[CrossRef](#)] [[PubMed](#)]
167. Chen, D.; Liu, C.; Chen, S.; Shen, W.; Luo, X.; Guo, L. Controlled Synthesis of Recyclable, Porous FMO/C@ TiO_2 Core-Shell Nanofibers with High Adsorption and Photocatalysis Properties for the Efficient Treatment of Dye Wastewater. *ChemPlusChem* **2016**, *81*, 282–291. [[CrossRef](#)]
168. Botes, M.; Eugene Cloete, T. The potential of nanofibers and nanobiocides in water purification. *Crit. Rev. Microbiol.* **2010**, *36*, 68–81. [[CrossRef](#)] [[PubMed](#)]
169. Tong, T.; Shereef, A.; Wu, J.; Binh, C.T.T.; Kelly, J.J.; Gaillard, J.-F.; Gray, K.A. Effects of Material Morphology on the Phototoxicity of Nano- TiO_2 to Bacteria. *Environ. Sci. Technol.* **2013**, *47*, 12486–12495. [[CrossRef](#)] [[PubMed](#)]
170. Djuricic, A.B.; Leung, Y.H.; Ching Ng, A.M. Strategies for improving the efficiency of semiconductor metal oxide photocatalysis. *Mater. Horiz.* **2014**, *1*, 400–410. [[CrossRef](#)]
171. Matsunaga, T.; Tomoda, R.; Nakajima, T.; Wake, H. Photoelectrochemical sterilization of microbial cells by semiconductor powders. *FEMS Microbiol. Lett.* **1985**, *29*, 211–214. [[CrossRef](#)]
172. He, J.; Wang, W.; Shi, W.; Cui, F. La_2O_3 nanoparticle/polyacrylonitrile nanofibers for bacterial inactivation based on phosphate control. *RSC Adv.* **2016**, *6*, 99353–99360. [[CrossRef](#)]
173. Lubasova, D.; Netravali, A.; Parker, J.; Ingel, B. Bacterial Filtration Efficiency of Green Soy Protein Based Nanofiber Air Filter. *J. Nanosci. Nanotechnol.* **2014**, *14*, 4891–4898. [[CrossRef](#)] [[PubMed](#)]
174. Macagnano, A.; Zampetti, E.; Bearzotti, A.; de Cesare, F. Electrospinning for Air Pollution Control. In *Electrospinning for Advanced Energy and Environmental Applications*; Cavaliere, S., Ed.; CRC Press: Boca Raton, FL, USA, 2015; pp. 243–280.
175. Tang, W.; Liu, G.; Li, D.; Liu, H.; Wu, X.; Han, N.; Chen, Y. Design and synthesis of porous non-noble metal oxides for catalytic removal of VOCs. *Sci. China Chem.* **2015**, *58*, 1359–1366. [[CrossRef](#)]
176. Huang, Z.-M.; Zhang, Y.-Z.; Kotaki, M.; Ramakrishna, S. A review on polymer nanofibers by electrospinning and their applications in nanocomposites. *Compos. Sci. Technol.* **2003**, *63*, 2223–2253. [[CrossRef](#)]
177. Fang, J.; Niu, H.; Lin, T.; Wang, X. Applications of electrospun nanofibers. *Chin. Sci. Bull.* **2008**, *53*, 2265. [[CrossRef](#)]
178. Lu, P.; Ding, B. Applications of Electrospun Fibers. *Recent Pat. Nanotechnol.* **2008**, *2*, 169–182. [[CrossRef](#)] [[PubMed](#)]
179. Liao, Y.; Fukuda, T.; Wang, S. Electrospun Metal Oxide Nanofibers and Their Energy Applications. In *Nanofiber Research—Reaching New Heights*; Rahman, M.M., Asiri, A.M., Eds.; InTech: Rijeka, Croatia, 2016.
180. Drew, C.; Liu, X.; Ziegler, D.; Wang, X.; Bruno, F.F.; Whitten, J.; Samuelson, L.A.; Kumar, J. Metal Oxide-Coated Polymer Nanofibers. *Nano Lett.* **2003**, *3*, 143–147. [[CrossRef](#)]
181. Dumitriu, C.; Stoian, A.B.; Titorencu, I.; Pruna, V.; Jinga, V.V.; Latonen, R.-M.; Bobacka, J.; Demetrescu, I. Electrospun TiO_2 nanofibers decorated Ti substrate for biomedical application. *Mater. Sci. Eng. C* **2014**, *45*, 56–63. [[CrossRef](#)] [[PubMed](#)]
182. Sabba, D.; Agarwala, S.; Pramana, S.S.; Mhaisalkar, S. A maskless synthesis of TiO_2 -nanofiber-based hierarchical structures for solid-state dye-sensitized solar cells with improved performance. *Nanoscale Res. Lett.* **2014**, *9*, 14. [[CrossRef](#)] [[PubMed](#)]
183. Horzum, N.; Tascioglu, D.; Ozbek, C.; Okur, S.; Demir, M.M. VOC sensors based on a metal oxide nanofibrous membrane/QCM system prepared by electrospinning. *New J. Chem.* **2014**, *38*, 5761–5768. [[CrossRef](#)]

184. Wang, X.; Gittens, R.A.; Song, R.; Tannenbaum, R.; Olivares-Navarrete, R.; Schwartz, Z.; Chen, H.; Boyan, B.D. Effects of structural properties of electrospun TiO₂ nanofiber meshes on their osteogenic potential. *Acta Biomater.* **2012**, *8*, 878–885. [[CrossRef](#)] [[PubMed](#)]
185. Wang, L.; Yu, Y.; Chen, P.-C.; Chen, C.-H. Electrospun carbon–cobalt composite nanofiber as an anode material for lithium ion batteries. *Scr. Mater.* **2008**, *58*, 405–408. [[CrossRef](#)]
186. Kim, J.-C.; Kim, D.-S.; Yeo, I.-H.; Kim, D.-W. Highly Porous Electrospun ZnCo₂O₄ Nanofibers for Lithium Ion Battery Electrodes. In Proceedings of the 229th ECS Meeting, San Diego, CA, USA, 29 May–2 June 2016; p. 315.
187. Ali, M.A.; Mondal, K.; Jiao, Y.; Oren, S.; Xu, Z.; Sharma, A.; Dong, L. Microfluidic Immuno-Biochip for Detection of Breast Cancer Biomarkers Using Hierarchical Composite of Porous Graphene and Titanium Dioxide Nanofibers. *ACS Appl. Mater. Interfaces* **2016**, *8*, 20570–20582. [[CrossRef](#)] [[PubMed](#)]
188. Liu, W.; Wei, J.; Chen, Y. Electrospun poly(L-lactide) nanofibers loaded with paclitaxel and water-soluble fullerenes for drug delivery and bioimaging. *New J. Chem.* **2014**, *38*, 6223–6229. [[CrossRef](#)]
189. Xiong, H.-M. ZnO Nanoparticles Applied to Bioimaging and Drug Delivery. *Adv. Mater.* **2013**, *25*, 5329–5335. [[CrossRef](#)] [[PubMed](#)]
190. Amna, T.; Hassan, M.S.; Nam, K.-T.; Bing, Y.Y.; Barakat, N.A.; Khil, M.-S.; Kim, H.Y. Preparation, characterization, and cytotoxicity of CPT/Fe₂O₃-embedded PLGA ultrafine composite fibers: A synergistic approach to develop promising anticancer material. *Int. J. Nanomed.* **2012**, *7*, 1659–1670. [[CrossRef](#)] [[PubMed](#)]
191. Maiyalagan, T.; Sundaramurthy, J.; Kumar, P.S.; Kannan, P.; Opallo, M.; Ramakrishna, S. Nanostructured α-Fe₂O₃ platform for the electrochemical sensing of folic acid. *Analyst* **2013**, *138*, 1779–1786. [[CrossRef](#)] [[PubMed](#)]
192. Ali, M.A.; Mondal, K.; Wang, Y.; Jiang, H.; Mahal, N.K.; Castellano, M.J.; Sharma, A.; Dong, L. In situ integration of graphene foam–titanium nitride based bio-scaffolds and microfluidic structures for soil nutrient sensors. *Lab Chip* **2017**, *17*, 274–285. [[CrossRef](#)] [[PubMed](#)]
193. Singh, G.; Vanangamudi, A.; Prince, J.A. Filtration Medium with electrospun Metal Oxide Nanofiber Layer. Patent WO 2013158028 A1, 2013.
194. Taha, A.A. Direct synthesis of mesostructured carbon nanofibers decorated with silver-nanoparticles as a multifunctional membrane for water treatment. *Adv. Nat. Sci. Nanosci. Nanotechnol.* **2015**, *6*, 045003. [[CrossRef](#)]
195. Homaeigohar, S.; Elbahri, M. Nanocomposite Electrospun Nanofiber Membranes for Environmental Remediation. *Materials* **2014**, *7*, 1017–1045. [[CrossRef](#)]
196. Zhang, X.; Liu, H.; Zheng, B.; Lin, Y.; Liu, D.; Nan, C.-W. Photocatalytic and Magnetic Behaviors Observed in BiFeO₃ Nanofibers by Electrospinning. *J. Nanomater.* **2013**, *2013*, 1–7.
197. Zhang, R.; Wu, H.; Lin, D.; Pan, W. Photocatalytic and Magnetic Properties of the Fe-TiO₂/SnO₂ Nanofiber Via Electrospinning. *J. Am. Ceram. Soc.* **2010**, *93*, 605–608. [[CrossRef](#)]
198. Santala, E.; Kemell, M.; Leskelä, M.; Ritala, M. The preparation of reusable magnetic and photocatalytic composite nanofibers by electrospinning and atomic layer deposition. *Nanotechnology* **2009**, *20*, 035602. [[CrossRef](#)] [[PubMed](#)]



© 2017 by the author. Licensee MDPI, Basel, Switzerland. This article is an open access article distributed under the terms and conditions of the Creative Commons Attribution (CC BY) license (<http://creativecommons.org/licenses/by/4.0/>).